UNIVERSIDAD DE CONCEPCIÓN

Centro de Investigación en Ingeniería Matemática (CI^{2}MA)

Computational uncertainty quantification for some strongly degenerate parabolic convection-diffusion equations

Raimund Bürger, Ilja Kröker

PREPRINT 2017-19

SERIE DE PRE-PUBLICACIONES

Computational uncertainty quantification for some strongly degenerate parabolic convection-diffusion equations

Raimund Bürger[a], Ilja Kröker[b,*]

[a] *CI²MA and Departamento de Ingeniería Matemática, Facultad de Ciencias Físicas y Matemáticas, Universidad de Concepción, Casilla 160-C, Concepción, Chile*
[b] *IANS, Universität Stuttgart, Pfaffenwaldring 57, D-70569 Stuttgart, Germany*

Abstract

Strongly degenerate parabolic convection-diffusion equations arise as governing equations in a number of applications such as traffic flow with driver reaction and anticipation distance and sedimentation of solid-liquid suspensions in mineral processing and wastewater treatment. In these applications certain parameters that define the convective flux function and the degenerating diffusion coefficient are subject to stochastic variability. A method to efficiently evaluate the variability of the solution of the governing partial differential equation in response to that of the parameters is presented. To this end, a general polynomial chaos (gPC) expansion of the solution is approximated by its projection onto a finite-dimensional space of piecewise polynomial functions defined on a suitable discretization of the stochastic domain, according to the basic principle of the hybrid stochastic Galerkin (HSG) approach. This approach is combined with a finite volume (FV) method, resulting in a so-called FV-HSG method, to compute the sought deterministic coefficient functions of the truncated polynomial-chaos-based expansion of the solution. Since the stochastic parameter space is now spanned by piecewise polynomial functions, one may employ the numerical result to compute the reconstruction of the numerical solution for arbitrary values of the random variables. The expectation, the variance or other stochastic quantities of the solution (as functions of time and position) can also be computed from these coefficient functions. The method is illustrated by a number of numerical examples.

Keywords: clarifier-thickener model, polynomial chaos, uncertainty quantification, traffic modelling, hybrid stochastic Galerkin, finite volume method

1. Introduction

1.1. Scope

This work is focused on numerical methods for the quantification of the stochastic variability of solutions $u = u(x,t)$ of the strongly degenerate parabolic equation

$$\partial_t u + \partial_x f(u) = \partial_x^2 A(u), \quad (x,t) \in Q_T := I \times (0,T), \quad T > 0, \tag{1}$$

that arises from uncertainty in the parameters that define the function $a = a(u)$, where

$$A(u) = \int_0^u a(s)\,\mathrm{d}s, \quad a \in L^1[0, u_{\max}], \quad a(u) \geq 0 \quad \text{for } 0 \leq u \leq u_{\max}. \tag{2}$$

Here the x-interval is either $I = \mathbb{R}$ corresponding to an initial value problem, or $I = (0,1)$, for which (1) is posed with suitable initial and boundary conditions. We assume that f is a piecewise smooth, Lipschitz

*Corresponding author
Email addresses: rburger@ing-mat.udec.cl (Raimund Bürger), ikroeker@mathematik.uni-stuttgart.de (Ilja Kröker)

continuous, non-negative function with support on $(0, u_{\max})$, where $u_{\max}$ is a maximum solution value. We allow that $a(u) = 0$ on u-intervals of positive lengths, which motivates why (1) is called *strongly degenerate*. For the u-values such that $a(u) = 0$, (1) degenerates into the first-order conservation law

$$\partial_t u + \partial_x f(u) = 0, \tag{3}$$

where the location of the type change interface is unknown beforehand. Consequently, solutions of (1) are in general discontinuous, and must be defined as weak solutions along with an entropy condition, that is, as entropy solutions.

Under the assumption of strong degeneracy, (1) arises in a number of applications, including a model of vehicular traffic with reaction times and anticipation lengths [8, 29, 30] and a model of sedimentation of flocculated suspensions [10, 13]. In both applications, it is frequently assumed that

$$a(u) \begin{cases} = 0 & \text{for } u \leq u_{\mathrm{c}} \text{ and } u > u_{\max}, \\ > 0 & \text{for } u_{\mathrm{c}} < u < u_{\max}, \\ \geq 0 & \text{for } u = u_{\max}, \end{cases} \tag{4}$$

where $u_{\mathrm{c}} \geq 0$ is a given critical value, so that (1) degenerates into (3) wherever $u \leq u_{\mathrm{c}}$. The value of u_{c} is, however, problem-dependent and usually not based on first principles. It either estimates the "threshold" value of the density u beyond which nonlinear diffusive effects become significant (a motivation that is common in traffic flow modeling) or represents a "phenomenological" parameter that characterizes geometrically complicated behaviour (such a the formation of a porous network formed by sedimentation of flocculated, non-spherical particles). In any case, the value of u_{c} is subject to uncertainty, and there is theoretical and practical interest in quantifying the uncertainty in the solution of (1) in terms of that of u_{c} and other parameters that arise in the algebraic definition of $a(u)$. It is the purpose of this contribution to provide an efficient computational method to solve this task. To this end, we introduce an appropriate definition of several random parameters, which represent uncertainty in the model problems. Based on this definition we provide the hybrid stochastic Galerkin (HSG) discretization for uncertain strongly parabolic degenerate problems. The HSG method is an intrusive stochastic Galerkin discretization method that was successfully applied to several non-linear hyperbolic problems, for example in [4, 12]. In general, intrusive SG discretizations transform the underlying partial differential equation (PDE), which is assumed to depend on random parameters, into a deterministic system by means of a Galerkin projection onto the stochastic space. We present an appropriate numerical scheme, which is based on central upwind method, and apply it to several examples motivated by real-world applications. Moreover, we study the accuracy of the method in short- and long-time numerical simulations and also the influence of the several random parameters on expectation and variance of the solution.

1.2. Related work

To put the present paper into the proper perspective, we mention that the applications motivating strongly degenerate parabolic equation (1), (2), namely traffic flow and sedimentation of flocculated suspensions, are broadly discussed in [1, 8, 29, 30, 34] and [13, 14], respectively (see also references cited in these papers). For the application to sedimentation, (1) equipped with initial and zero-flux boundary conditions describes the simple process of batch settling in a column, but the same functions f and A also arise in more involved models of continuous sedimentation in clarifier-thickener models, in which the governing PDE (not written out here) includes additional transport terms accounting for bulk flows, singular source terms, and discontinuous coefficients (see [7, 10, 16] and references cited in these papers). The usefulness of (1) as a practical model for real-world phenomena depends critically on calibration, that is, the possibility to identify the model functions f and A (or equivalently, a) for real situations. These issues are addressed in [1] and [6, 17, 15, 38] for the models of traffic flow and sedimentation, respectively. The present work deals with a closely related issue, namely the assessment of the variability of the model prediction in response to the uncertainty in constitutive model functions. Another problem that arises for clarifier-thickener models with

time-dependent control functions lies in the fact that there is not only uncertainty in the appropriate choice of material specific constitutive functions (as is considered herein), but that also many input parameters that represent time-dependent operating conditions cannot be described with deterministic accuracy but by stochastic methods. For instance, in mineral processing the uncertainty comes from the fact that the feed flow stems from other units that are not under control of the CT operator, while in wastewater treatment weather conditions, which may affect the operation of the unit, are unpredictable. An HSG approach to computationally quantify the uncertainty arising in this situation was applied in [4, 11, 12].

With respect to uncertainty quantification for conservation laws and related partial differential equations in a general context, we mention that the straightforward Monte Carlo (MC) computations of sampling solutions produced under stochastic variation of the input data are easily implemented, but quantifying randomness via the MC approach can be computationally inefficient due to the slow convergence rate of stochastic approach, in particular in the case of high computational costs for each sample. However, the computational efficiency of MC can be significantly improved by multi-level Monte-Carlo [5, 28] and quasi-Monte-Carlo [20] techniques.

In this paper we focus on the hybrid stochastic Galerkin (HSG) discretization which belongs to the broad class of intrusive stochastic Galerkin (SG) methods. The application of the intrusive SG methods to the uncertainty quantification of PDEs goes back to the work by Ghanem and Spanos in the early 1990s [18, 27]. In the past decades several authors used several intrusive methods for uncertainty quantification of the random perturbed hyperbolic problems. In particular we would like to accent the work by Poëtte et al. [31] who discussed the well-posedness of the application of intrusive SG methods to non-linear random perturbed hyperbolic problems, and the work by Tryoen et al. [37] who introduced multi-wavelet stochastic discretization [2, 25] for hyperbolic problems.

As is mentioned above, the intrusive SG discretization was applied to the clarifier-thickener (CT) model with random feed in [11]. The HSG discretization and stochastic adaptivity for this discretization applied to the CT model were introduced in [12]. This method was extended in [4] to handle several random variables within the CT model with random feed.

1.3. Outline of this paper

The remainder of this paper is organized as follows. In Section 2 some preliminaries are collected. In this work we discuss three different initial-boundary value problems for (1) that are addressed as Problem A, B and C, respectively, and that differ by the choice of I and the boundary conditions, which are specified in Section 2.1. Problems A or B correspond to the diffusively corrected version of the Lighthill-Whitham-Richards (LWR) traffic model, which is summarized in Section 2.2, on an infinite or circular highway, while Problem C, with zero-flux boundary conditions, arises as a model of batch settling of a suspension of fine particles dispersed in a viscous fluid that form a compressible sediment. This model is summarized in Section 2.3. For each model we specify in Section 2.4 the parameters that are subject to stochastic variability.

In Section 3 we give a short overview on the HSG discretization. We start with an introduction to the general polynomial chaos (gPC) expansion (Section 3.1) and its extension to the HSG discretization (Section 3.2). Then, in Section 3.3 we apply the HSG method to the governing equation (1), and outline in Section 3.4 the finite volume method for the numerical approach. Section 3.5 summarises Section 3 and provides a brief overview of the motivation and computational aspects of the method.

In Section 4 we present several numerical experiments, based on settings provided in Section 2. We start with Section 4.1, where we specify several problem parameters that are used in the numerical examples. Example 1, presented in Section 4.2, treats the diffusively corrected LWR traffic model with random perturbations on infinite highway. In Section 4.3 we present Example 2, which considers the model above on a circular highway. Examples 3 to 5 in Sections 4.4 and 4.5 deal with a model of sedimentation of flocculated suspensions, where Section 4.4 handles the setting common for mineral processing, and we analyse in Section 4.5 long- and short-time simulations for the setting that is used in wastewater treatment. Finally, in Section 5 we recapitulate the results presented, analyse advantages and limitations of the presented method and provide an outlook on the future research. An appendix addresses the preservation of parabolicity for the HSG discretization.

2. Preliminaries

2.1. Initial and boundary conditions

For Problems A, B and C we always impose the initial condition

$$u(x,0) = u_0(x), \quad x \in I, \tag{5}$$

where Problem A corresponds to $I = \mathbb{R}$ and an initial value problem, and Problems B and C to $I = [0,1]$ with the following periodic conditions for Problem B:

$$u(0,t) = u(1,t) \quad \text{for } t > 0, \tag{6}$$

and zero-flux boundary conditions for Problem C, i.e.,

$$\big(f(u) - \partial_x A(u)\big)\big|_{x=0} = 0, \quad \big(f(u) - \partial_x A(u)\big)\big|_{x=1} = 0. \tag{7}$$

2.2. Diffusively corrected LWR traffic model

The classical LWR traffic model [26, 32] postulates that vehicular traffic on an infinite or circular highway can be modeled by Problem A or B, respectively, for the first-order conservation law (3), where u is the local density of cars that is assumed to vary between zero and a maximum value $u_{\max}$, and

$$f(u) = v_{\max} u V(u). \tag{8}$$

Here $v_{\max} > 0$ is a maximum freeway velocity and V is a decreasing function that satisfies $V(0) = 1$ and $V(u_{\max}) = 0$, and which describes drivers' attitude to reduce speed in presence of other cars. A common choice [19] is the function

$$V(u) = 1 - u/u_{\max}. \tag{9}$$

Numerous motifications of the original LWR model (3), (8) have been proposed. In particular, this model lacks realism in that the driver reaction of the vehicle located at position x at time t depends on the spot value $u(x,t)$ (instead of the density some "anticipation distance" L_{a} ahead), and that the reaction is instantaneous while in reality it would be delayed by a reaction time τ. These shortcomings are corrected in the modification of the LWR model advanced by Nelson [30] (see also [1, 8]) that includes the effects of anticipation distance and reaction time. The anticipation length L_{a} may depend on $V(u)$. In fact, the following formula is proposed in [30]:

$$L_{\mathrm{a}}(u) = \max\left\{\frac{(v_{\max} V(u))^2}{2\alpha}, L_{\min}\right\}, \tag{10}$$

where $L_{\min}$ is a minimal anticipation distance and α denotes a deceleration, so that the first argument in (10) denotes the distance required to decelerate from speed $V(u)$ to full stop at deceleration α. The velocity of a vehicle at position x at time t is no longer assumed to depend on the spot value $u(x,t)$, but rather on the density at position $x + L_{\mathrm{a}} - V\tau$ at time $t - \tau$. By an appropriate expansion of u evaluated at this displaced argument around (x,t) [8, 30] we obtain that to within an $\mathcal{O}(\tau^2 + L_{\mathrm{a}}^2)$ error in consistency, $u = u(x,t)$ is now given by (1) (instead of (3)) with A given by (2), where

$$a(u) = -u v_{\max} V'(u)\big(L_{\mathrm{a}}(u) + \tau u v_{\max} V'(u)\big). \tag{11}$$

In [1, 8, 30] it is proposed to utilize a particular function V (alternative to (9)) that satisfies $V(u) = \text{const.}$ for $u < u_*$, where $0 < u_* < u_{\max}$, such that in view of (11), the strongly degenerate behaviour (4) holds for $u_{\mathrm{c}} := u_*$ and $u = u_{\max}$. Herein we assume, however, that independently of the algebraic definition of V, the critical value u_{c} is a prescribed "psycho-physiological" threshold value in the sense that reaction times and anticipation lengths are assumed to be effective only whenever the local traffic density u exceeds u_{c} (see [34]). Consequently, our analysis will be based on the following formula:

$$a(u) = \begin{cases} 0 & \text{for } u \le u_{\mathrm{c}}, \\ -u v_{\max} V'(u)\big(L_{\mathrm{a}}(u) + \tau u v_{\max} V'(u)\big) & \text{for } u > u_{\mathrm{c}}. \end{cases} \tag{12}$$

2.3. Settling of a suspension forming compressible sediments

Problem C describes the settling of a suspension of fine particles dispersed in a viscous fluid, where u denotes the local solids concentration in depth x at time t. The convective flux f is again given by (8), where $v_{\max}$ now denotes the settling velocity of a single particle in an unbounded fluid and the function V describes the effect of hindrance to settling exerted by other particles. Common formulas are the Richardson-Zaki expression [33] (widely used in mineral processing)

$$V(u) = (1-u)^{n_{\mathrm{RZ}}}, \quad n_{\mathrm{RZ}} > 1, \tag{13}$$

where n_{RZ} is a material-dependent exponent, and the Vesilind formula [39] (common in wastewater treatment)

$$V(u) = \exp(-r_{\mathrm{V}} u), \qquad \text{where } r_{\mathrm{V}} > 0 \text{ is a parameter.} \tag{14}$$

According to a well-studied sedimentation-consolidation model [10, 14], the diffusion function is given by

$$a(u) = \frac{V(u)\sigma_{\mathrm{e}}'(u)}{\Delta\rho g}, \tag{15}$$

where $\sigma_{\mathrm{e}}'(u) := \mathrm{d}\sigma_{\mathrm{e}}/\mathrm{d}u$ is the derivative of the effective solid stress function, $\Delta\rho > 0$ is the solid-fluid density difference, and g is the acceleration of gravity. It is assumed that the effective solid stress can only be transmitted wherever particles touch each other and form a porous network, which is assumed to occur whenever u exceeds a critical concentration or gel point u_{c}, and that σ_{e} is an increasing function of u whenever $u > u_{\mathrm{c}}$. Consequently, the diffusion coefficient $a(u)$ defined by (15) satisfies (4). A widely used formula for σ_{e} in mineral processing is the power law

$$\sigma_{\mathrm{e}}(u) = \begin{cases} 0 & \text{for } u \le u_{\mathrm{c}}, \\ \sigma_0\big((u/u_{\mathrm{c}})^k - 1\big) & \text{for } u > u_{\mathrm{c}}, \end{cases} \quad \sigma_0 = 0, \quad k > 0, \tag{16}$$

while the following expression is more common in wastewater treatment [7, 15]:

$$\sigma_{\mathrm{e}}(u) = \begin{cases} 0 & \text{for } u \le u_{\mathrm{c}}, \\ \sigma_0 \ln\big(1 + (u-u_{\mathrm{c}})/\beta\big) & \text{for } u > u_{\mathrm{c}}, \end{cases} \quad \sigma_0 = 0, \quad \beta > 0. \tag{17}$$

Thus, will discuss either the diffusion coefficient suitable for mineral processing (where V is given by (13)),

$$a(u) = \begin{cases} 0 & \text{for } u \le u_{\mathrm{c}}, \\ \dfrac{v_{\max} V(u) \sigma_0 k}{\Delta\rho g u_{\mathrm{c}}^k} u^{k-1} & \text{for } u > u_{\mathrm{c}}, \end{cases} \tag{18}$$

or the diffusion coefficient appropriate for wastewater treatment, where V is given by (14):

$$a(u) = \begin{cases} 0 & \text{for } u \le u_{\mathrm{c}}, \\ \dfrac{v_{\max} V(u) \sigma_0 \rho_u}{\Delta\rho g(\beta + u - u_{\mathrm{c}})} & \text{for } u > u_{\mathrm{c}}. \end{cases} \tag{19}$$

2.4. Stochastic variability

We assume that the parameters arising in $a(u)$ in the traffic model and both variant of the sedimentation model are subject to stochastic variability while in all cases the parameters $v_{\max}$ and the function V are given. For a unified treatment we denote the parameters arising in (12) by

$$p_1 = u_{\mathrm{c}}, \quad p_2 = \tau, \quad p_3 = \alpha, \quad p_4 = L_{\min}, \tag{20}$$

those of (18) by,

$$p_1 = u_c, \quad p_2 = \sigma_0, \quad p_3 = k, \tag{21}$$

and those of (19) by

$$p_1 = u_c, \quad p_2 = \sigma_0, \quad p_3 = \beta. \tag{22}$$

We wish to assess the uncertainty in the solution of Problem A or B (for the traffic model) and of Problem C (for the sedimentation model) under the assumption that the stochastic variability of a number N of parameters $p_1, \ldots, p_N$ is specified by

$$p_i = \bar{p}_i \left(1 + \left(\theta_i - \frac{1}{2}\right) \sigma_i\right) \quad i = 1, \ldots, N_s,$$

where N denotes the total number of parameters that are subject to random variability, $\bar{p}_i$ the mean value of p_i, θ_i is a random variable that is uniformly distributed on $(0,1)$ ($\theta_i \sim \mathcal{U}(0,1)$), and σ_i measures the variation of p_i, all for $i = 1, \ldots, N_s$. Here we consider the cases $1 \le N_s \le 4$.

3. Hybrid stochastic Galerkin (HSG) discretization

3.1. General polynomial chaos (gPC) expansion

Let $\boldsymbol{\theta}(\boldsymbol{\omega}) := (\theta_1(\omega_1), \ldots, \theta_{N_s}(\omega_{N_s})^T$ be an N_s–dimensional random vector of i.i.d. (independent identically distributed) random variables defined on the probability spaces $(\Omega_i, \mathcal{F}_i, \mathcal{P}_i)$, $i = 1, \ldots, N_s$. We define a multivariate polynomial $\Phi_{\mathfrak{p}}$ for a multi-index $\mathfrak{p} \in \mathbb{N}^{N_s}$ by

$$\Phi_{\mathfrak{p}}(\boldsymbol{\omega}) := \phi_{\mathfrak{p}_1}(\theta_1) \cdot \ldots \cdot \phi_{\mathfrak{p}_{N_s}}(\theta_{N_s}).$$

The choice of the orthonormal polynomial $\phi_{\mathfrak{p}_i}$, $\mathfrak{p}_i \in \mathbb{N}_0$ depends on the law of the random variable θ_i. In the present work we assume that the random variables are uniformly distributed $\theta_i \sim \mathcal{U}(0,1)$ and therefore use re-scaled Legendre polynomials. The family of the multivariate polynomials $\{\Phi_{\mathfrak{p}}\}_{\mathfrak{p} \in \mathbb{N}_0^{N_s}}$ is orthonormal with respect to the scalar product on $L^2(\Omega^{N_s})$, i.e.,

$$\langle \Phi_{\mathfrak{p}}, \Phi_{\mathfrak{q}} \rangle_{L^2(\Omega^{N_s})} := \int_{\Omega_1} \cdots \int_{\Omega_{N_s}} \Phi_{\mathfrak{p}}(\boldsymbol{\theta}(\boldsymbol{\omega})) \Phi_{\mathfrak{q}}(\boldsymbol{\theta}(\boldsymbol{\omega})) \, \mathrm{d}\mathcal{P}_1(\omega_1) \cdots \mathcal{P}_{N_s}(\omega_{N_s}) = \delta_{\mathfrak{p}\mathfrak{q}}.$$

Furthermore, the polynomial chaos expansion of a random variable with finite variance $w = w(x, t, \boldsymbol{\theta}(\boldsymbol{\omega}))$, $(x,t) \in \mathbb{R} \times [0,T]$, $\boldsymbol{\omega} \in \Omega^{N_s}$ is given by

$$w\big(x,t,\boldsymbol{\theta}(\boldsymbol{\omega})\big) = \sum_{q=0}^{\infty} \sum_{|\mathfrak{p}|=q} w^{\mathfrak{p}}(x,t) \Phi_{\mathfrak{p}}(\boldsymbol{\theta}(\boldsymbol{\omega})), \quad \text{where } w^{\mathfrak{p}}(x,t) := \langle w(x,t,\cdot), \Phi_{\mathfrak{p}} \rangle_{L^2(\Omega^N)} \tag{23}$$

for $(x,t) \in \mathbb{R} \times [0,T]$, $\boldsymbol{\omega} \in \Omega^{N_s}$. Truncating the infinite series (23) by summing over $|\mathfrak{p}| \le N_o$ leads to a finite sum of $(N_o + N_s)!/(N_o! N_s!)$ terms. This observation will be applied when constructing the truncation within the HSG discretization.

3.2. Extension to HSG discretization

The main idea of the HSG method is the decomposition of the stochastic domain $[0,1]^{N_s}$ (we assume $\theta_i \sim \mathcal{U}(0,1)$) into the following $2^{N_s N_r}$ sub-domains, where $N_r \in \mathbb{N}_0$:

$$I^{N_r}_{N_s,l} := I^{N_r}_{l_1} \times \cdots \times I^{N_r}_{l_{N_s}}, \; l = (l_1, \ldots, l_{N_s}) \in \mathcal{I} := \left\{0, \ldots, 2^{N_r} - 1\right\}^{N_s}.$$

Here we define the intervals

$$I_{l_i}^{N_\mathrm{r}} := [2^{-N_\mathrm{r}} l_i, 2^{-N_\mathrm{r}}(l_i+1)], \quad l_i = 0, \ldots, 2^{N_\mathrm{r}} - 1.$$

The space of the multivariate piecewise polynomial functions $S_{N_\mathrm{s}}^{N_\mathrm{o},\,N_\mathrm{r}}$ is given by

$$S_{N_\mathrm{s}}^{N_\mathrm{o},\,N_\mathrm{r}} := \left\{ w : [0,1]^{N_\mathrm{s}} \to \mathbb{R} \;\middle|\; w|_{I_{N_\mathrm{s},l}^{N_\mathrm{r}}} \in \mathbb{Q}_{N_\mathrm{o}}^{N_\mathrm{s}}[\boldsymbol{\theta}],\ \forall l \in \mathcal{I} \right\}.$$

Here $\mathbb{Q}_{N_\mathrm{o}}^{N_\mathrm{s}}[\boldsymbol{\theta}]$ denotes the space of N_s-variate polynomials of degree $\leq N_\mathrm{o}$. The basis of the space $S_{N_\mathrm{s}}^{N_\mathrm{o},\,N_\mathrm{r}}$ can be given by the polynomials

$$\Phi_{\mathfrak{p},l}^{N_\mathrm{r}}(\boldsymbol{\theta}) := \begin{cases} 2^{N_\mathrm{s}N_\mathrm{r}/2} \Pi_{k=1}^{N_\mathrm{s}} \phi_{\mathfrak{p}_k}(2^{N_\mathrm{r}}\theta_k - l_k) & \text{for } \boldsymbol{\theta} \in I_{N_\mathrm{s},l}^{N_\mathrm{r}}, \\ 0 & \text{otherwise,} \end{cases} \quad \text{for } \mathfrak{p} \in \mathbb{N}_0^{N_\mathrm{s}},\ |\mathfrak{p}| \leq N_\mathrm{o},\ l \in \mathcal{I}, \tag{24}$$

where $\{\phi_k\}_{k\geq 0}$ are the re-scaled orthonormal Legendre polynomials. Therefore also the N_s-variate polynomials (24) satisfy the orthogonality relation

$$\left\langle \Phi_{\mathfrak{p},l}^{N_\mathrm{r}},\, \Phi_{\mathfrak{q},k}^{N_\mathrm{r}} \right\rangle_{L^2(\Omega^{N_\mathrm{s}})} = \delta_{\mathfrak{p}\mathfrak{q}}\delta_{lk}, \quad \text{for } \mathfrak{p},\mathfrak{q} \in \mathbb{N}_0^{N_\mathrm{s}},\ k,l \in \mathcal{I}. \tag{25}$$

Similarly to the gPC expansion in the previous section we define the projection

$$\Pi^{N_\mathrm{o},N_\mathrm{r}} : L^2(\Omega^{N_\mathrm{s}}) \to S_{N_\mathrm{s}}^{N_\mathrm{r},\,N_\mathrm{o}}$$

of the random variable $w(x,t,\boldsymbol{\theta}(\boldsymbol{\omega})) \in L^2(\Omega^{N_\mathrm{s}})$ for $(x,t) \in \mathbb{R} \times [0,T]$ onto the space of the multivariate piecewise polynomial functions $S_{N_\mathrm{s}}^{N_\mathrm{r},\,N_\mathrm{o}}$ by

$$\Pi^{N_\mathrm{o},N_\mathrm{r}}[w](x,t,\boldsymbol{\theta}) := \sum_{l\in\mathcal{I}} \sum_{|\mathfrak{p}|\leq N_\mathrm{o}} w_{\mathfrak{p},l}^{N_\mathrm{r}}(x,t)\Phi_{\mathfrak{p},l}^{N_\mathrm{r}}(\boldsymbol{\theta}), \quad w_{\mathfrak{p},l}^{N_\mathrm{r}} := \left\langle w,\, \Phi_{\mathfrak{p},l}^{N_\mathrm{r}} \right\rangle_{L^2(\Omega^{N_\mathrm{s}})} \quad \text{for } l \in \mathcal{I},\ \mathfrak{p} \in \mathbb{N}_0^{N_\mathrm{s}}. \tag{26}$$

This projection allows us to represent the random variable $w(x,t,\boldsymbol{\theta})$ by the vector of deterministic coefficients $w_{\mathfrak{p},l}^{N_\mathrm{r}}(x,t)$ for $l \in \mathcal{I}$, $\mathfrak{p} \in \mathbb{N}_0^{N_\mathrm{s}}$, which are associated with appropriate multivariate piecewise polynomial functions in $S_{N_\mathrm{s}}^{N_\mathrm{r},\,N_\mathrm{o}}$. The convergence of $\Pi^{N_\mathrm{o},N_\mathrm{r}}$ for $N_\mathrm{r}, N_\mathrm{o} \to \infty$ was shown in [3]. Due to the assumptions on the random variable w, the expectation and variance of $\Pi^{N_\mathrm{o},N_\mathrm{r}}[w]$ can be computed as follows:

$$\mathbf{E}\left[\Pi^{N_\mathrm{o},N_\mathrm{r}}[w]\right](x,t) := \sum_{l\in\mathcal{I}} w_{0,l}^{N_\mathrm{r}}(x,t) \left\langle \Phi_{0,l}^{N_\mathrm{r}},\, \Phi_{0,0}^{0} \right\rangle_{L^2(\Omega^{N_\mathrm{s}})}, \tag{27}$$

$$\mathbf{Var}\left[\Pi^{N_\mathrm{o},N_\mathrm{r}}[w]\right](x,t) := \sum_{l\in\mathcal{I}} \sum_{|\mathfrak{p}|\leq N_\mathrm{o}} w_{\mathfrak{p},l}^{N_\mathrm{r}}(x,t)^2 - \left(\mathbf{E}\left[\Pi^{N_\mathrm{o},N_\mathrm{r}}[w]\right](x,t)\right)^2. \tag{28}$$

3.3. Application of the HSG approach to the governing equation

In order to apply the HSG approach to the final model we replace the unknown u in (1), (2) by its projection onto $S_{N_\mathrm{s}}^{N_\mathrm{r},\,N_\mathrm{o}}$ for N_s, N_r, $N_\mathrm{o} \in \mathbb{N}_0$, denoted by $\Pi^{N_\mathrm{o},N_\mathrm{r}}[u]$. The HSG approach of the equation (1), (2) reads as follows: find coefficients $u_{\mathfrak{p},l}^{N_\mathrm{r}} : \mathbb{R} \times [0,T] \to \mathbb{R}$ such that

$$\int_{\Omega^{N_\mathrm{s}}} \left(\Pi^{N_\mathrm{o},N_\mathrm{r}}[u]_t + f\left(\Pi^{N_\mathrm{o},N_\mathrm{r}}[u]\right)_x - A\left(\Pi^{N_\mathrm{o},N_\mathrm{r}}[u]\right)_{xx} \right) \Phi_{\mathfrak{p},l}^{N_\mathrm{r}} \,\mathrm{d}\mathcal{P}(\boldsymbol{\omega}) = 0$$

$$\text{for all } (\mathfrak{p},l) \in \mathbb{N}_0^{N_\mathrm{s}} \times \mathcal{I},\ |\mathfrak{p}| \leq N_\mathrm{o}.$$

By using the orthogonality relation (25) we obtain for $(x,t,\boldsymbol{\omega}) \in \mathbb{R} \times (0,T] \times \Omega^{N_\mathrm{s}}$, $\alpha = (\mathfrak{p},l) \in \mathbb{N}_0^{N_\mathrm{s}} \times \mathcal{I}$, $|\mathfrak{p}| \leq N_\mathrm{o}$ the system

$$u_t^\alpha + \left(\left\langle f\left(\Pi^{N_\mathrm{o},N_\mathrm{r}}[u]\right),\, \Phi_\alpha \right\rangle_{L^2(\Omega^{N_\mathrm{s}})} \right)_x = \partial_x^2 \left\langle A\left(\Pi^{N_\mathrm{o},N_\mathrm{r}}[u]\right),\, \Phi_\alpha \right\rangle_{L^2(\Omega^{N_\mathrm{s}})} \tag{29}$$

of dimension

$$M := 2^{N_\mathrm{s}N_\mathrm{r}} \frac{(N_\mathrm{o}+N_\mathrm{s})!}{N_\mathrm{o}!N_\mathrm{s}!}. \tag{30}$$

3.4. Finite volume method

The central-upwind scheme was introduced in [24] and successfully used together with an HSG discretization in [12, 21, 22]. For the numerical approach we extend that scheme by a second-order term and obtain for $j \in \mathbb{Z}$ the following numerical scheme in semi-discrete form:

$$\frac{\mathrm{d}}{\mathrm{d}t}\bar{\boldsymbol{U}}_{j+1/2}(t) = -\frac{1}{\Delta x}\big(\boldsymbol{F}_{j+1}(t) - \boldsymbol{F}_j(t)\big) + \frac{1}{\Delta x^2}\big(\boldsymbol{A}(\bar{\boldsymbol{U}}_{j+3/2}(t)) - 2\boldsymbol{A}(\bar{\boldsymbol{U}}_{j+1/2}(t)) + \boldsymbol{A}(\bar{\boldsymbol{U}}_{j-1/2}(t))\big),$$

where we define the numerical flux

$$\boldsymbol{F}_j(t) := \frac{a_j^+ \boldsymbol{f}(\boldsymbol{U}_j^+) + a_j^- \boldsymbol{f}(\boldsymbol{U}_j^-)}{a_j^+ + a_j^-} + \frac{a_j^+ a_j^-}{a_j^+ + a_j^-}\left(\boldsymbol{U}_j^+ - \boldsymbol{U}_j^-\right).$$

The so-called local speeds $a_j^\pm$ are derived from the Jacobian of $\boldsymbol{f}$, we refer to [23, 24, 40] for details. Moreover, the cell averages on $[x_j, x_{j+1}]$, denoted by $\bar{\boldsymbol{U}}_{j+1/2}$, and the piecewise polynomial reconstructions denoted by $\boldsymbol{U}_j^\pm$ are given by

$$\bar{\boldsymbol{U}}_{j+1/2} = \big(\bar{u}^0_{j+1/2}, \dots, \bar{u}^{M-1}_{j+1/2}\big)^{\mathrm{T}} \quad \text{and} \quad \boldsymbol{U}_j^\pm = \big((u_j^\pm)^0, \dots, (u_j^\pm)^{M-1}\big)^{\mathrm{T}}.$$

The piecewise polynomial reconstructions $(u_j^\pm)^\alpha$ for $\alpha = 0, \dots, M-1$ (cf. (30)) are defined by

$$(u_j^+)^\alpha := \bar{u}^\alpha_{j+1/2} - \frac{\Delta x}{2} r^\alpha_{j+1/2}, \quad (u_j^-)^\alpha := \bar{u}^\alpha_{j-1/2} + \frac{\Delta x}{2} r^\alpha_{j-1/2},$$

where

$$r^\alpha_{j+1/2} := \operatorname{minmod}\left(s\frac{\bar{u}^\alpha_{j+1/2} - \bar{u}^\alpha_{j-1/2}}{\Delta x}, \frac{\bar{u}^\alpha_{j+3/2} - \bar{u}^\alpha_{j-1/2}}{2\Delta x}, s\frac{\bar{u}^\alpha_{j+3/2} - \bar{u}^\alpha_{j+1/2}}{\Delta x}\right), \ s \in [1, 2],$$

and we use the standard minmod function defined by

$$\operatorname{minmod}(a, b, c) = \begin{cases} \operatorname{sgn}(a)\min\{|a|, |b|, |c|\} & \text{if } \operatorname{sgn}(a) = \operatorname{sgn}(b) = \operatorname{sgn}(c), \\ 0 & \text{otherwise.} \end{cases}$$

The vectors $\boldsymbol{f}(\boldsymbol{U}_j)$ and $\boldsymbol{A}(\boldsymbol{U}_j)$ are given by

$$\boldsymbol{f}(\boldsymbol{U}_j) = \big(f^0(\boldsymbol{U}_j), \dots, f^{M-1}(\boldsymbol{U}_j)\big)^{\mathrm{T}}, \quad \boldsymbol{A}(\boldsymbol{U}_j) = \big(A^0(\boldsymbol{U}_j), \dots, A^{M-1}(\boldsymbol{U}_j)\big)^{\mathrm{T}},$$

where we define

$$f^\alpha(\boldsymbol{U}_j) := \left\langle f\left(\sum_{\beta=0}^{M-1} u_j^\beta \Phi_\beta\right), \Phi_\alpha \right\rangle_{L^2(\Omega^{N_\mathrm{s}})}, \qquad A^\alpha(\boldsymbol{U}_j) := \left\langle A\left(\sum_{\beta=0}^{M-1} u_j^\beta \Phi_\beta\right), \Phi_\alpha \right\rangle_{L^2(\Omega^{N_\mathrm{s}})}.$$

The time discretization is given by the second-order Runge-Kutta/Heun method defined by

$$U^{n+1} = \frac{1}{2}U^n + \frac{1}{2}\left(U^* + \Delta t L[U^*]\right), \quad U^* = U^n + \Delta t L[U^n].$$

Here U^n is the unknown variable at the n-th time-step, $L[U]$ the spatial operator, which is supposed to provide a second order approach of $\mathcal{L}[U]$, solving $U_t = \mathcal{L}[U]$. For more details, see e.g. [35].

	Examples 1 and 2			Example 3			Example 4			Example 5		
i	p_i	$\bar{p}_i$	σ_i	p_i	$\bar{p}_i$	σ_i	p_i	$\bar{p}_i$	σ_i	p_i	$\bar{p}_i$	σ_i
1	u_c [cars/km]	10.0	0.25	u_c [−]	0.2	0.1	u_c [kg/m^3]	5	0.1	u_c [kg/m^3]	5	0.02
2	τ [s]	2.0	0.25	σ_0 [Pa]	50	0.2	σ_0 [Pa]	7	0.02	σ_0 [Pa]	7	0.1
3	α [m/s^2]	9.81×10^{-4}	0.5	k [−]	6	1/3	β [kg/m^3]	2.9	0.02	β [kg/m^3]	2.9	0.1
4	L_min [km]	0.08	0.125	——			——			——		

Table 1: Examples 1 to 5: randomly perturbed parameters.

3.5. Summary of the method of computational uncertainty quantification

We conclude the analysis by a summary of the method of computational uncertainty quantification. The purpose of the method is to provide an efficient tool to numerically investigate the influence of several random parameters within the coefficients of the governing PDE (1) on the unknown solution u. The unknown solution u is considered as a random variable, which is represented by their projection onto the space of piecewise polynomial functions defined in (26). Precisely speaking, the goal of the method is to compute the deterministic coefficient functions $u_{\mathfrak{p},l}^{N_\mathrm{r}}(x,t)$ that determine the projection $\Pi^{N_\mathrm{o},N_\mathrm{r}}[u]$ of the unknown u, defined by (26) for $w = u$ with u satisfying (29), for all indices $|\mathfrak{p}| \leq N_\mathrm{o}$, $l \in \mathcal{I}$. Since the stochastic parameter space is spanned by the piecewise polynomial functions in $S_{N_\mathrm{s}}^{N_\mathrm{o},N_\mathrm{r}}$, this procedure allows us to compute the reconstruction of the numerical approach of $u(x,t,\boldsymbol{\theta})$ for $(x,t) \in \mathbb{R} \times [0,T]$ and an arbitrary choice of $\boldsymbol{\theta} \in [0,1]^{N_\mathrm{s}}$ by evaluation of $\Pi^{N_\mathrm{o},N_\mathrm{r}}[u]$ on $(x,t,\boldsymbol{\theta})$.

The usual quantities of interest in stochastic applications, namely the expectation and the variance, can be also computed from the coefficient functions $u_{\mathfrak{p},l}^{N_\mathrm{r}}$ by application of formulas (27) and (28), respectively. The other quantities of interest, for example higher stochastic moments, can also be computed by using the orthogonality of the polynomials $\{\Phi_{\mathfrak{p},l}^{N_\mathrm{r}}\}_{l\in\mathcal{I},\,|\mathfrak{p}|\leq N_\mathrm{o}}$ or computing of the reconstructions of the approximate solution for an appropriate choice of the random parameters $\boldsymbol{\theta} \in [0,1]^{N_\mathrm{s}}$.

4. Numerical examples

4.1. Preliminaries

In the numerical examples we apply the FV-HSG method presented in the previous section to different scenarios. We compute the numerical solutions for several maximal polynomial orders N_o and resolution N_r at the end time T. For the spatial discretization of the interval I use an equidistant mesh with 200 subintervals.

For the analysis of the accuracy of the stochastic discretization we compare the expectation and variance at time T computed with the FV-HSG method with the corresponding quantities of the reference solution. To analyze the error in the approach of the expectation and variance we use spatial L^1 and L^2 norms for the expectation and L^2 and L^4 norms for the variance, respectively.

The reference solution in each case is the result of the MC approach with 10^5 samples, where each sample is a deterministic solution of the problem (1), (2) for a randomly chosen parameter set $\boldsymbol{\theta} \in [0,1]^{N_\mathrm{s}}$ computed by the scalar version of the finite volume method which was introduced in the Sec. 3.4.

4.2. Example 1: Model 1/Problem A

In Example 1, vehicular traffic on an infinite highway is modelled by the random perturbed diffusively corrected LWR traffic model on the interval $I = [0, 5.6]$ (Problem A in Sect. 2.1). For the traffic model (Model 1) we use the function (8) with $v_\mathrm{max} = 100\,\mathrm{km/h} = 2.78 \times 10^{-2}\,\mathrm{m/s}$. The density u is measured in cars per kilometer, and we assume that $u_\mathrm{max} = 120\,\mathrm{cars/km}$. The critical density is set to $u_\mathrm{c} = 10\,\mathrm{cars/km}$. The remaining parameters are similar to those used in [1, 8] for the reaction and anticipation terms, namely $\alpha = 0.1g = 0.981\,\mathrm{m/s^2}$, where g is the acceleration of gravity, $\tau = 2\,\mathrm{s}$, and $L_\mathrm{min} = 80\,\mathrm{m}$.

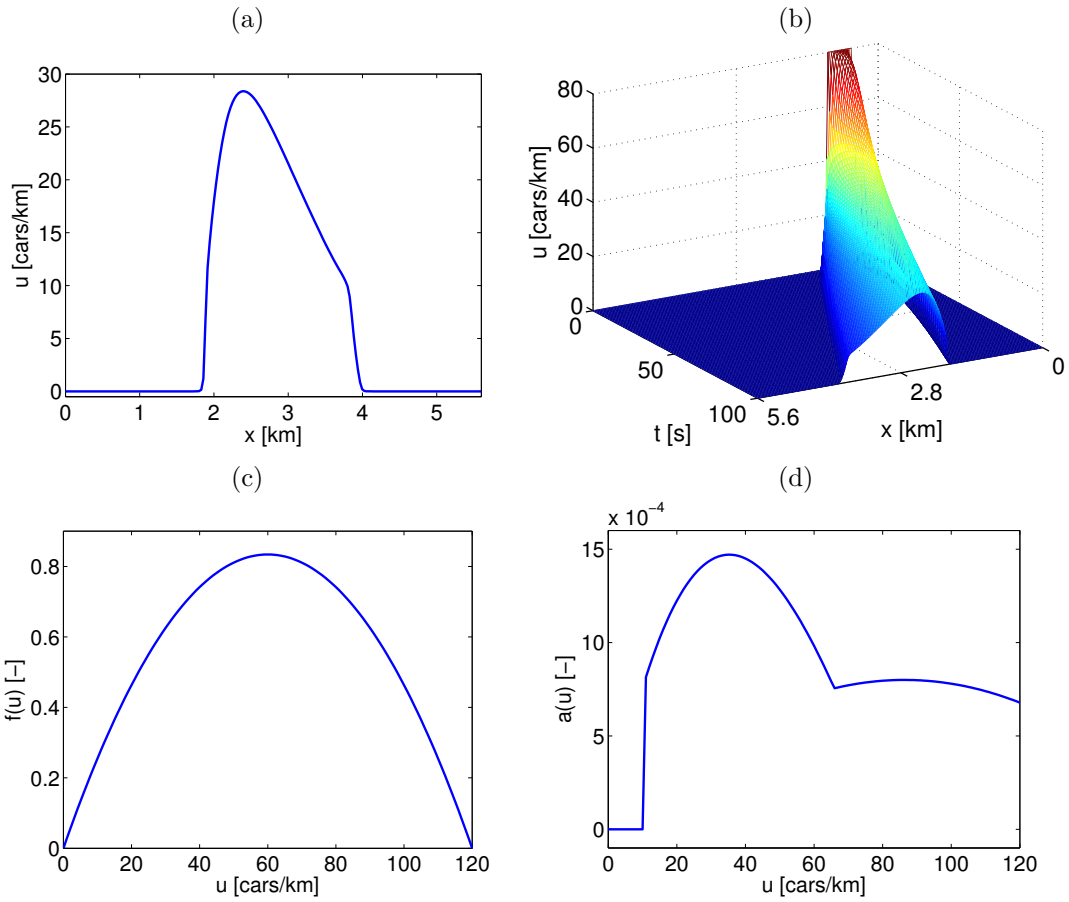

Figure 1: Example 1 (Model 1/Problem A): numerical solution for $T = 100\,\mathrm{s}$, computed with the central-upwind scheme: (a) deterministic solution; (b) time series of the deterministic solution for $t \in [0, T]$; (c) $f(u)$ for $u \in [0, 120]$; (d) $a(u)$ for $u \in [0, 120]$.

The initial distribution is given by

$$u_0(x) := \begin{cases} 80\,\mathrm{cars/km} & \text{if } 2.0 \le x \le 2.5\,\mathrm{km}, \\ 0\,\mathrm{cars/km} & \text{otherwise.} \end{cases} \tag{31}$$

The problem parameters that are subject to stochastic variability mentioned in Table 1.

The interval I is subdivided into $N = 200$ subintervals, and we simulate until a final time $T = 100\,\mathrm{s}$. The numerical results are computed with the FV-HSG method with $N_\mathrm{r} = 0, \ldots, 2$, $N_\mathrm{o} = 0, \ldots, 2$. Figure 2 (a) shows the expectation and the variance at $t = T$. Figure 2 (b) shows reconstructions of the numerical solution for ten parameter sets at $t = T$. These reconstructions illustrate the dependence of the solution on the possible random perturbed parameter values and explain the shape of the plot of the variance in Figure 2 (a). Figures 2 (c) and (d) show the evolution of the expectation and variance of the numerical solution for $t \in [0, 100]$. Figures 2 (e) and (f) show expectation and variance computed with several choices of N_r and N_o compared with MC solution. Table 2 shows the L^1- and L^2-errors for the expectation and L^2- and L^4-errors for the variance of the FV-HSG approach compared with the MC solution.

The numerical approach of expectation and variance with the FV-HSG method shows the convergence for increasing N_r in all norms considered, where the convergence for lower maximal polynomial order N_o is faster, then for the higher order. In particular, the method provides a good approach of the expectation also

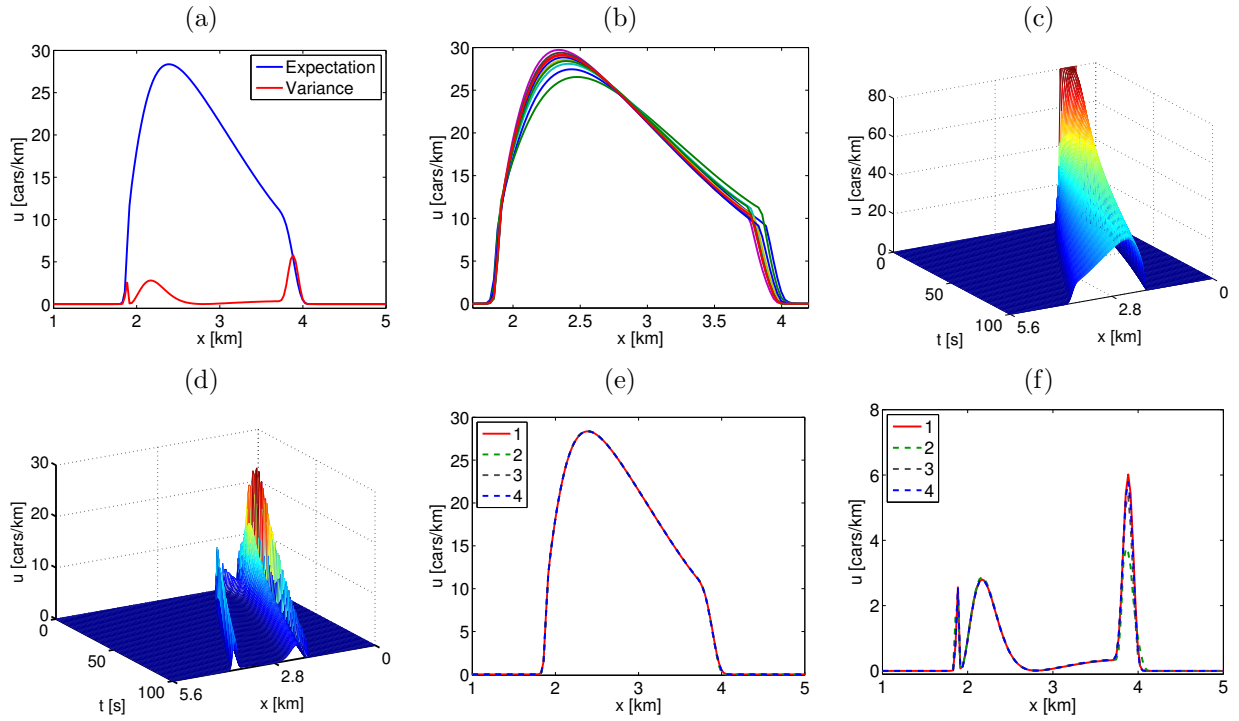

Figure 2: Example 1 (Model 1/Problem A): numerical solution for $T = 100\,\mathrm{s}$ computed with the central-upwind and FV-HSG schemes for $N_\mathrm{r} = 2$, $N_\mathrm{o} = 2$: (a) expectation and variance; (b) reconstructions for 10 different parameter sets; (c) expectation of the solution for $t \in [0, T]$; (d) variance of the solution for $t \in [0, T]$; (e, f) comparisons of (e) expectations and (f) variances: (1) MC, (2) HSG with $N_\mathrm{r} = 0$, $N_\mathrm{o} = 2$, (3) HSG with $N_\mathrm{r} = 1$, $N_\mathrm{o} = 2$, (4) HSG with $N_\mathrm{r} = 2$, $N_\mathrm{o} = 2$.

for the lower accuracy of the stochastic discretization. In the approach of the variance we have also general good match away from the peaks caused by the convection part of the equation, which shows an appropriate matching only for $N_\mathrm{r} \geq 1$.

4.3. Example 2: Model 1/Problem B

We now simulate the vehicular traffic on a circular highway modelled by the diffusively corrected LWR traffic model. The circular highway is modeled by the interval $I = [0, 1]$ km with periodic boundary conditions (Problem B). The initial distribution is given by

$$u_0(x) := \begin{cases} 80\,\mathrm{cars/km} & \text{if } 0.25 \leq x \leq 0.5\,\mathrm{km}, \\ 0\,\mathrm{cars/km} & \text{otherwise.} \end{cases} \tag{32}$$

The parameters used in the simulation and those that are perturbed randomly are the same as in Example 1, see Table 1. The numerical solution for the deterministic setting at $t = T$ and also the evolution for $t \in [0, T]$ are shown in Figure 3.

The numerical results for the random perturbed problem are shown in Figure 4. In particular, Figure 4 (a) shows expectation variance computed by the FV-HSG method with $N_\mathrm{r} = 2$, $N_\mathrm{o} = 2$ at $T = 100$ s. The reconstructions for ten parameter sets at $t = T$ from the HSG representation with $N_\mathrm{r} = 2$ and $N_\mathrm{o} = 2$ are presented in Figure 4 (b). The evolution of the expectation and variance computed with FV-HSG with $N_\mathrm{r} = 2$, $N_\mathrm{o} = 2$ for $t \in [0, T]$ is presented in Figures 4 (c) and (d), respectively. Figures 4 (e) and (f) show the comparison of the FV-HSG numerical solution for several choices of N_r and N_o with the reference solution.

		Expectation						Variance					
		L^1 error			L^2 error FV-HSG/MC			L^2 error			L^4 error FV-HSG/MC		
	N_o	$N_r=0$	$N_r=1$	$N_r=2$	$N_r=0$	$N_r=1$	$N_r=2$	$N_r=0$	$N_r=1$	$N_r=2$	$N_r=0$	$N_r=1$	$N_r=2$
Example 1	0	2.63e-1	6.64e-2	1.72e-2	2.54e-1	5.92e-2	1.50e-2	2.48e+0	5.78e-1	1.39e-1	3.26e+0	7.51e-1	1.75e-1
	1	1.19e-1	5.38e-2	2.26e-2	1.35e-1	5.49e-2	2.31e-2	7.76e-1	2.58e-1	9.82e-2	1.18e+0	4.36e-1	1.67e-1
	2	1.11e-1	6.06e-2	2.81e-2	1.20e-1	6.11e-2	2.60e-2	7.18e-1	2.66e-1	1.04e-1	1.19e+0	4.55e-1	1.76e-1
Example 2	0	3.85e-2	9.20e-3	2.34e-3	4.29e-2	1.02e-2	2.59e-3	4.76e-2	1.25e-2	3.14e-3	6.02e-2	1.57e-2	3.96e-3
	1	2.42e-3	1.42e-3	6.87e-4	3.01e-3	1.71e-3	8.40e-4	2.67e-3	6.09e-4	1.47e-4	3.16e-3	8.06e-4	1.85e-4

Table 2: Examples 1 and 2 (Model 1, Problems A and B): Expectation: (a) L^1-error, (b) L^2-error of the FV-HSG approach compared with MC. Variance: (c) L^2-error, (d) L^4-error of the FV-HSG approach compared with MC.

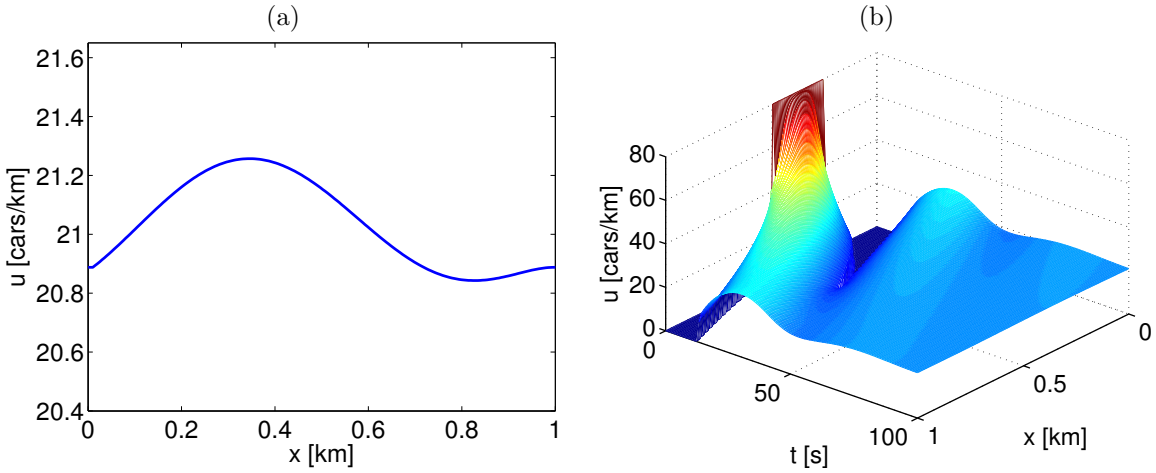

Figure 3: Example 2 (Model 1/Problem B): numerical solution of the deterministic problem computed with the central-upwind scheme: (a) numerical solution at $T = 100$; (b) time series of the numerical solution for $t \in [0, T]$.

Table 2 shows L^1 and L^2 error of the expectation and L^2 and L^4 error of the variance for $N_r = 0, \ldots, 2$ and $N_o = 0, 1$.

The numerical experiments show the convergence of the expectation and variance for increasing N_r. The highest difference between reconstructions of the several parameter sets corresponds to the maximum of the variance. Similar to the Example 1 the method provides fair accuracy for the approach of the expectation also for the lower N_r, but the proper approach of the variance requires higher computational accuracy ($N_r \geq 1$).

4.4. Example 3: Model 2/Problem C

Examples 3 to 5 are related to the settling of a suspension forming compressible sediment. The sedimentation model will be used in two versions (Model 2 (Example 3) and Model 3 (Examples 4 and 5)). Model 2 is based on the assumptions stated in [9] that are typical for mineral processing. In that setting u is assumed to denote a volume fraction, assuming values between zero and one, and we assume that f is given by (8) with $v_{\max} = 10^{-4}\,\mathrm{m/s}$ and V is given by (14) with $r_V = 6\,\mathrm{m^3/kg}$. Here the diffusion coefficient is given by (18), where the effective solid stress function σ_e is defined by (16) with $\sigma_0 = 50\,\mathrm{Pa}$, $u_c = 0.2$ and $k = 6$. Other parameters are $g = 9.81\,\mathrm{m/s^2}$ and $\Delta\rho = 1500\,\mathrm{kg/m^3}$.

We use the zero-flux boundary conditions (Problem C in Sect. 2.1). The initial distribution $u_0(\cdot)$ on the

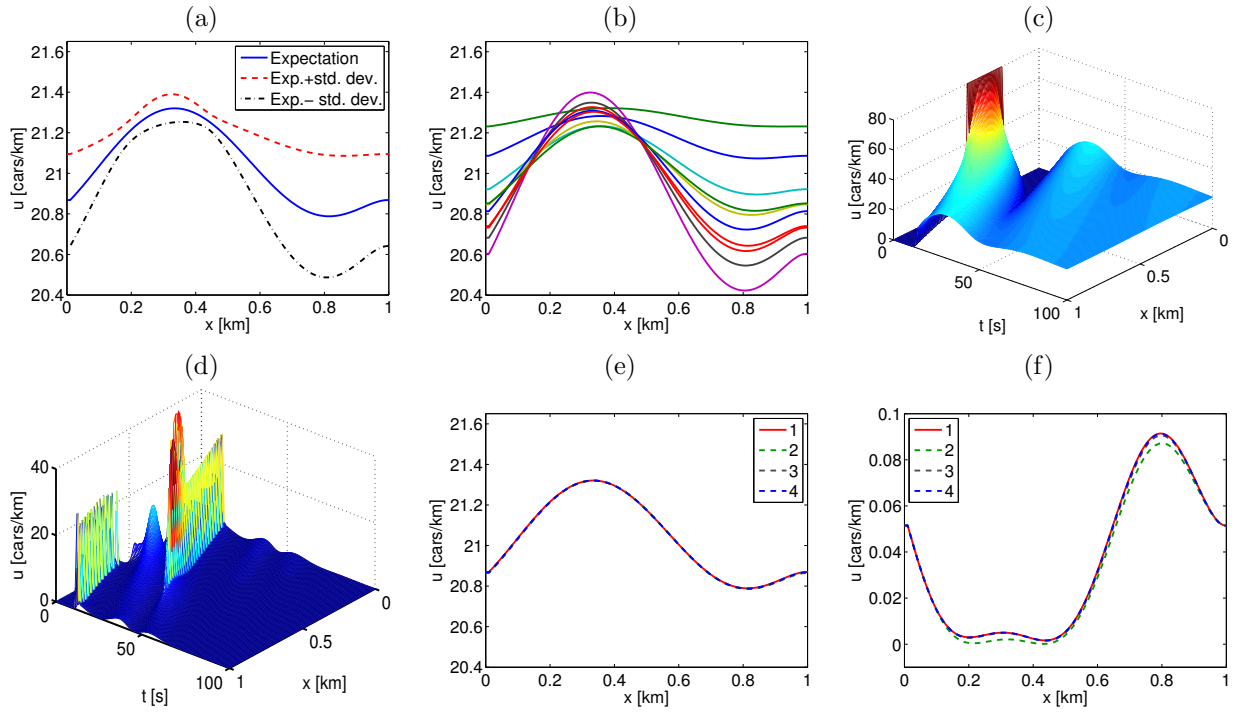

Figure 4: Example 2 (Model 1/Problem B): numerical results for $T = 100\,\mathrm{s}$ computed with central-upwind and FV-HSG schemes for $N_\mathrm{r} = 2$, $N_\mathrm{o} = 1$: (a) expectation and variance; (b) reconstructions for 10 several parameter sets; (c) expectation of the solution for $t \in [0, T]$; (d) variance of the solution for $t \in [0, T]$; (e, f) comparison of (e) expectations and (f) variances (f): (1) MC, (2) HSG with $N_\mathrm{r} = 0$, $N_\mathrm{o} = 1$, (3) HSG with $N_\mathrm{r} = 1$, $N_\mathrm{o} = 1$, (4) HSG with $N_\mathrm{r} = 2$, $N_\mathrm{o} = 1$.

interval I is given by

$$u_0(x) := \begin{cases} 0.85 & \text{if } 0.5 \le x \le 0.6, \\ 0 & \text{otherwise.} \end{cases} \tag{33}$$

The parameters that are subject to stochastic variability are indicated in Table 1.

The numerical solution at $t = T$ of the deterministic version of the problem, the evolution for $t \in [0, T]$, the flux function $f(u)$, its derivative $f'(u)$, and the diffusion coefficient $a(u)$ are shown in Figure 5. The results of the application of the FV-HSG method on the random perturbed problem with three random parameters are shown in the Fig. 6. In particular Fig. 6 (a) shows the expectation and variance at $T = 1.5 \times 10^4$. Figure 6 (b) shows the reconstructions for ten parameter sets. Figures 6 (c) and (d) show the evolutions of the expectation and and variance for $t \in [0, T]$.

For the analysis of accuracy of the stochastic discretization we compare the expectation and variance computed with FV-HSG with $N_\mathrm{r} = 0, \ldots, 3$, $N_\mathrm{o} = 0, 1$ with the both moments computed with MC. Figures 6 (e) and (f) show the corresponding plots, and Table 3 shows the error of the approach.

The comparison of the numerical approach of expectation and variance computed with FV-HSG with the reference solution indicates convergence for increasing N_r. Nevertheless the high variability of shape of the solution with respect to the choice of random parameter $\boldsymbol{\theta}$, in particular position of the shock, requires to use the higher N_r to achieve an accurate numerical solution.

4.5. Examples 4 and 5 (Model 3/Problem C)

The parameters of Model 3 (Examples 4 and 5) are chosen more closely to assumptions typical in wastewater treatment. In that application, and in our examples, u is measured in $\mathrm{kg/m^3}$. We adopt the parameters

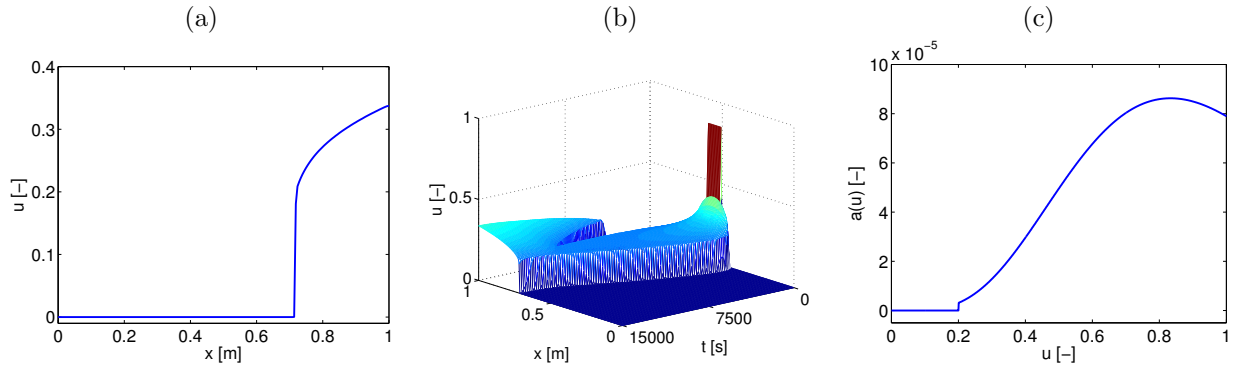

Figure 5: Example 3 (Model 2/Problem C): (a) deterministic solution at $t = T = 15000\,\mathrm{s}$ computed with the central-upwind scheme; (b) time series for $t \in [0, T]$; (c) comparison of $f(u)$, $f'(u)$ and $a(u)$ for $u \in [0, 1]$.

employed in [7]. The function f is given by (8) with $v_{\max} = 6.336\,\mathrm{m/h} = 1.76 \times 10^{-3}\,\mathrm{m/s}$ and V is given by (14) with $r_V = 0.55\,\mathrm{m^3/kg}$. The effective solid stress function σ_e is defined by (17) with $\sigma_0 = 7\,\mathrm{Pa}$, $u_c = 5\,\mathrm{kg/m^3}$ and $\beta = 2.9\,\mathrm{kg/m^3}$. The diffusion function a is then given by (18) with $g = 9.81\,\mathrm{m/s^2}$, $\rho_u = 1050\mathrm{kg/m^3}$ and $\Delta\rho = 52\,\mathrm{kg/m^3}$.

In Examples 4 and 5 we investigate the short- and long-time influence of the magnitude of the random parameters controlled by σ_i, $i = 1, 2, 3$ on the settling of a suspension forming compressible sediments introduced in the Sect. 2.3. Here the diffusion coefficient is given by (19). We use zero-flux boundary conditions (Problem C). The initial distribution is given by

$$u_0(x) := \begin{cases} 10\,[\mathrm{kg/m^3}] & \text{if } 0.25\,\mathrm{m} \le x \le 0.5\,\mathrm{m}, \\ 0 & \text{otherwise.} \end{cases} \tag{34}$$

Examples 4 and 5 differ in the specification of the random parameters (see Table 1). The short- and the long- time behaviour of the deterministic numerical solution for $t = 200\,\mathrm{s}$ and $t = T = 2500\,\mathrm{s}$, respectively is shown in Figure 7. The flux function $f(u)$, derivative of the flux function $f'(u)$ and the diffusion coefficient $a(u)$ for $u \in [0, 40]$ are shown in Figure 7 (e).

For the discussion of the short-time behaviour of the numerical solution we apply the FV-HSG method to Examples 4 and 5 at $t = 200\,\mathrm{s}$ for $N_r = 0, \ldots, 3$, $N_o = 0, \ldots, 2$. Figures 8 and 9 show the expectation, variance, reconstructions for ten parameter sets and also comparison with the MC results for first and second settings respectively. Table 3 shows L^1- and L^2- error for the expectation and L^2- and L^4 error for the variance. For tests of the accuracy we use the MC result as the reference solution.

In the next step we study the long-time behaviour of the numerical solution. For this purpose we apply the FV-HSG method to both Examples 4 and 5 at $T = 2500$ for $N_r = 0, \ldots, 3$, $N_o = 0, 1$. Figures 10 and 11 show the expectation, variance, reconstructions for ten parameter sets and also the comparison with the MC results. Table 3 displays the L^1- and L^2-errors for the expectation and L^2- and L^4-error for the variance.

The numerical experiments have shown that the magnitude of the random perturbations of the diffusion threshold parameter u_c have a strongest influence on the short- and also the long- time behaviour of the numerical solution. This can also be concluded from the comparison of the variances of the numerical solutions for Examples 4 and 5. In both examples it can be observed that the position of the highest variance correlates with the uncertain position of the shock. The numerical approach of expectation and variance with the FV-HSG method shows convergence for increasing N_r in all considered norms in both examples. In particular in the test case with higher variance of the solution the FV-HSG approach shows the slightly higher accuracy for $N_o = 2$ than for $N_o = 1$ also for higher N_r.

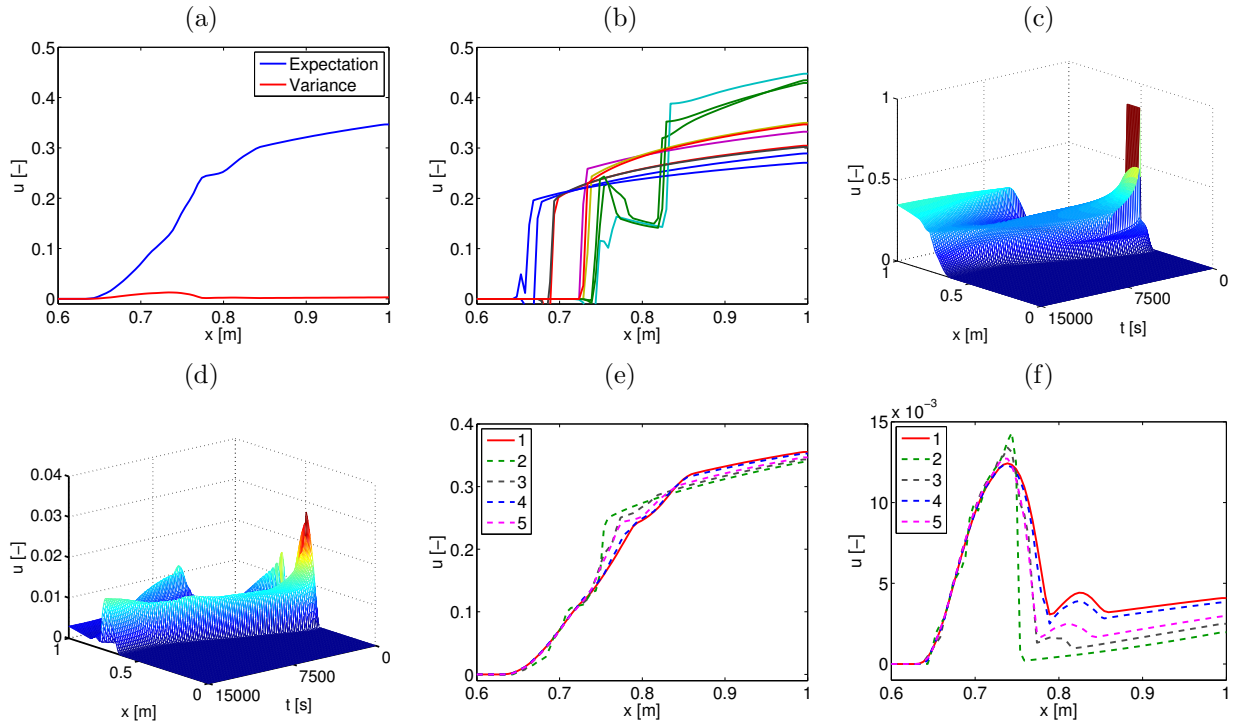

Figure 6: Example 3 (Model 2/Problem C): numerical solution for $T = 1.5 \times 10^4$ computed with central-upwind and FV-HSG scheme for $N_\mathrm{r} = 3$, $N_\mathrm{o} = 1$: (a) expectation and variance; (b) reconstructions for 10 several parameter sets; (c) expectation of the solution for $t \in [0, T]$; (d) variance of the solution for $t \in [0, T]$; (e, f) comparison of (e) expectations and (f) variances: (1) MC; (2) HSG with $N_\mathrm{r} = 1$, $N_\mathrm{o} = 1$; (3) HSG with $N_\mathrm{r} = 2$, $N_\mathrm{o} = 1$; (4) HSG with $N_\mathrm{r} = 3$, $N_\mathrm{o} = 0$; (5) HSG with $N_\mathrm{r} = 3$, $N_\mathrm{o} = 1$.

5. Conclusions

In this work we applied the FV-HSG method to several scenarios (motivated by traffic modelling, mineral processing and wastewater treatment) that are modelled by the non-linear parabolic strongly degenerate equation (1) with $N_\mathrm{s} = 3$ or $N_\mathrm{s}) = 4$ random parameters. The numerical challenge of the problem is the complicated definition of the diffusion term that requires adaptive time-stepping and evaluation of the numerical quadrature over the stochastic space in each time step. We have presented the HSG discretization of the model problems and introduced a corresponding numerical scheme. Several examples illustrate the utility of the FV-HSG method for studying the expectation and variance of the numerical solution and also the influence of singular random parameters.

The short-time and long-time numerical experiments show the convergence of the expectation and variance computed with the FV-HSG method to the reference solution given by the MC approach for increasing polynomial order N_o for a low number of resolution N_r as well as for an increasing number of resolution N_r. It could be also observed that at least for the complex settings considered in Example 1, Tab. 2, a lower polynomial order N_o provides a higher accuracy for increasing N_r than a higher polynomial order N_o. The observation of the highest variance of the numerical solution usually correlates with the uncertain position of the shock front, which is also often the cause of the Gibbs phenomena in several polynomial-based UQ discretization methods. Nevertheless, the numerical artefacts caused by Gibbs phenomenon, which often appear in numerical simulations of non-linear hyperbolic problems discretized by classical SG, can be avoided for higher N_r.

One of the important advantages of the HSG method (and also of other intrusive methods) is the pos-

			N_o	$N_r=0$	$N_r=1$	$N_r=2$	$N_r=3$		N_o	$N_r=0$	$N_r=1$	$N_r=2$	$N_r=3$
Example 3	Expectation	(a)	0	1.60e-2	6.55e-3	2.24e-3	8.66e-4	(b)	0	3.21e-2	1.27e-2	4.76e-3	1.82e-3
$T=15000$			1	9.58e-3	6.85e-3	4.79e-3	3.32e-3		1	2.07e-2	1.53e-2	1.01e-2	7.36e-3
	Variance	(c)	0	3.77e-3	1.50e-3	6.14e-4	2.28e-4	(d)	0	6.05e-3	2.74e-3	1.13e-3	4.38e-4
			1	2.81e-3	2.02e-3	1.19e-3	9.51e-4		1	5.18e-3	3.95e-3	2.03e-3	1.78e-3
Example 4	Expectation	(a)	0	5.07e-2	2.29e-2	6.07e-3	6.44e-3	(b)	0	1.91e-1	9.22e-2	2.45e-2	3.38e-2
$T=200$			1	7.91e-2	3.22e-2	1.51e-2	5.31e-3		1	2.39e-1	9.49e-2	4.89e-2	2.36e-2
			2	7.63e-2	3.53e-2	1.10e-2	4.73e-3		2	2.33e-1	1.03e-1	3.65e-2	2.30e-2
	Variance	(c)	0	5.20e-1	2.22e-1	6.68e-2	8.16e-2	(d)	0	1.35e+0	5.27e-1	1.70e-1	2.43e-1
			1	3.13e-1	1.79e-1	1.12e-1	4.36e-2		1	7.47e-1	4.89e-1	2.98e-1	1.49e-1
			2	3.11e-1	1.89e-1	5.90e-2	4.22e-2		2	7.75e-1	5.14e-1	1.73e-1	1.48e-1
Example 4	Expectation	(a)	0	5.16e-2	2.30e-2	8.67e-3	9.89e-4	(b)	0	2.46e-1	1.15e-1	4.36e-2	5.08e-3
$T=2500$			1	2.65e-2	1.24e-2	3.51e-3	9.27e-4		1	1.36e-1	6.20e-2	1.76e-2	3.33e-3
	Variance	(c)	0	8.25e-1	3.28e-1	1.33e-1	5.15e-2	(d)	0	1.98e+0	9.25e-1	3.47e-1	1.24e-1
			1	3.56e-1	2.40e-1	8.92e-2	2.38e-2		1	9.15e-1	6.60e-1	2.50e-1	6.69e-2
Example 5	Expectation	(a)	0	5.76e-3	2.66e-3	2.06e-3	2.06e-3	(b)	0	2.72e-2	1.57e-2	1.43e-2	1.48e-2
$T=200$			1	1.48e-2	5.92e-3	2.79e-3	2.18e-3		1	7.07e-2	2.56e-2	1.64e-2	1.53e-2
			2	1.53e-2	5.10e-3	2.55e-3	2.14e-3		2	7.29e-2	2.35e-2	1.61e-2	1.53e-2
	Variance	(c)	0	6.61e-2	2.37e-2	2.42e-2	2.20e-2	(d)	0	2.15e-1	6.55e-2	7.22e-2	6.76e-2
			1	5.44e-2	2.78e-2	2.29e-2	2.27e-2		1	1.90e-1	8.85e-2	7.12e-2	7.09e-2
			2	5.28e-2	2.90e-2	2.34e-2	2.28e-2		2	1.86e-1	9.42e-2	7.33e-2	7.14e-2
Example 5	Expectation	(a)	0	8.16e-3	1.13e-3	3.00e-4	1.07e-4	(b)	0	7.08e-2	8.17e-3	2.48e-3	8.16e-4
T=2500			1	2.85e-3	6.83e-4	1.04e-4	4.51e-5		1	2.39e-2	3.56e-3	7.90e-4	3.47e-4
	Variance	(c)	0	2.34e-1	5.65e-2	1.16e-2	3.18e-3	(d)	0	8.15e-1	1.91e-1	4.14e-2	1.13e-2
			1	8.86e-2	2.48e-2	4.96e-4	1.04e-3		1	3.20e-1	8.44e-2	1.56e-3	3.86e-3

Table 3: Examples 3 to 5: (a) L^1-error, (b) L^2-error of the FV-HSG approach compared with MC. Variance: (c) L^2-error, (d) L^4-error of the FV-HSG approach compared with MC.

sibility to reconstruct the quantities of interest during post-processing without to consider them during the simulation, and also without the saving of all samples.

The main limitation of the method is the rapidly increasing computational complexity for increasing number of random parameters N_s. Nevertheless the partially decoupled structure of the HSG discretization allows efficient parallelization also on bigger clusters, because the effort for the synchronisation of data between stochastic elements $I^{N_r}_{N_s,l}$ during the simulation can be reduced to the minimum. Therefore the method can be efficiently implemented on MPI+OpenMP infrastructure and combined with stochastic adaptivity discussed in [4, 12].

Further improvements of the computational efficiency could be expected by using of load balancing tools particularly with regard to the different computational effort on different stochastic elements. Also the exploiting of the matrix vector structure is promising from the point of view of implementation for many core or GPU-based systems.

6. Appendix: Parabolicity of the HSG discretization

Let us consider the system (29) in the non-degenerate case. For $\boldsymbol{U} = \left(u^0, \dots, u^{M-1}\right)^{\mathrm{T}}$ the system (29) can be rewritten into

$$\boldsymbol{U}_t + B(\boldsymbol{U})\boldsymbol{U}_x = C(\boldsymbol{U})\boldsymbol{U}_{xx}, \quad \text{on } \mathbb{R} \times (0,T). \tag{35}$$

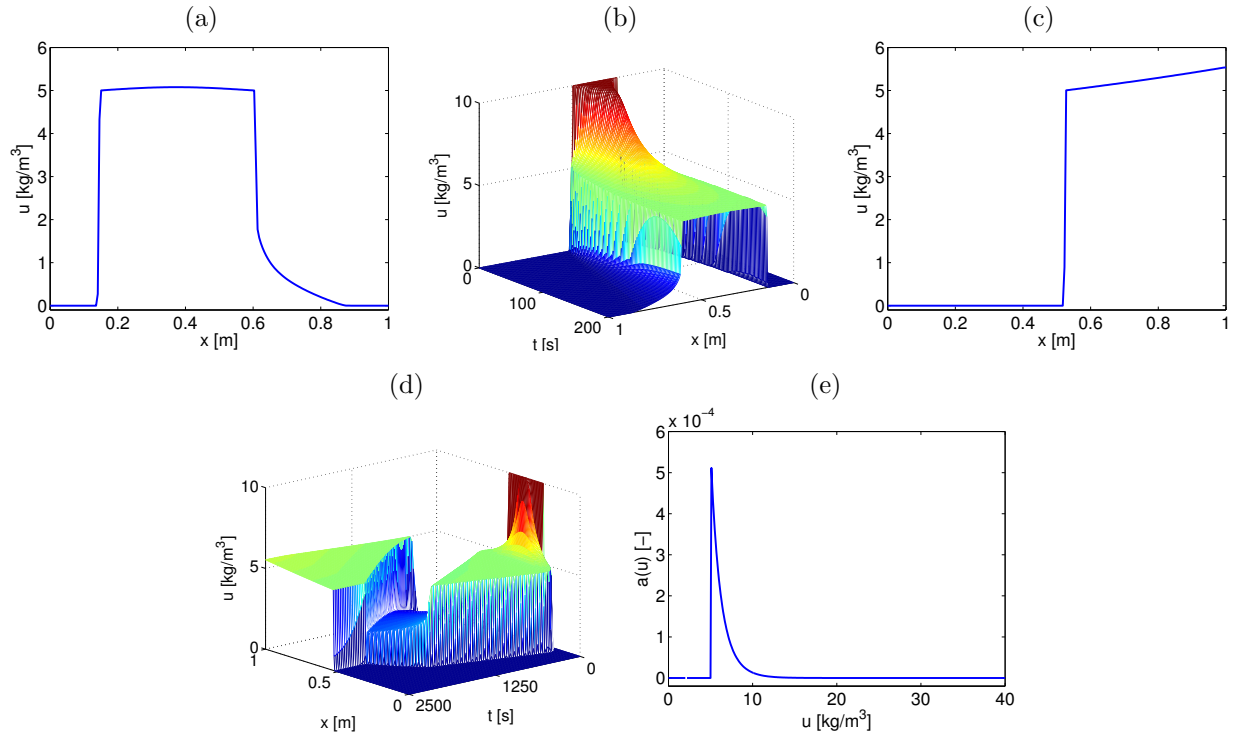

Figure 7: Example 4 (Model 3/Problem C): numerical solution computed with the central-upwind scheme (deterministic solution) (a) at $T = 200$; (b) time series for $t \in [0, 200]$; (c) at $T = 2500$; (d) time series for $t \in [0, 2500]$. (e) $a(u)$ for $u \in [0, 40]$.

Here the $M \times M$ matrices $B(\boldsymbol{U}) := (b_{\alpha\beta})$ and $C(\boldsymbol{U}) := (c_{\alpha\beta})$ are given by

$$b_{\alpha\beta} := \left\langle f'\left(\Pi^{N_o,N_r}[u]\right) - a'\left(\Pi^{N_o,N_r}[u]\right)\sum_{\gamma=0}^{M-1} u_x^{\gamma}\Phi_\gamma,\ \Phi_\alpha\Phi_\beta \right\rangle_{L^2(\Omega^{N_s})}$$

$$c_{\alpha\beta} := \left\langle a\left(\Pi^{N_o,N_r}[u]\right),\ \Phi_\alpha\Phi_\beta\right\rangle_{L^2(\Omega^{N_s})}.$$

It is easy to see, that the matrix $B(\boldsymbol{U})$ is symmetric. From the equation (4) we know that $a(u) \geq 0$ for all $u \in \mathbb{R}$. Therefore we can write $c_{\alpha\beta}$ as

$$c_{\alpha\beta} = \left\langle \sqrt{a\left(\Pi^{N_o,N_r}[u]\right)}\Phi_\alpha,\ \sqrt{a\left(\Pi^{N_o,N_r}[u]\right)}\Phi_\beta \right\rangle_{L^2(\Omega^{N_s})},$$

and obtain that $C(\boldsymbol{U})$ is a positive semi-definite Gram matrix. From the assumption of the non-degeneracy follows $a(u) > 0$ and also that the vectors

$$\left\{ \sqrt{a\left(\Pi^{N_o,N_r}[u]\right)}\Phi_\alpha \mid \alpha = 0, \ldots, M-1 \right\}$$

are linearly independent. In this case the matrix $C(\boldsymbol{U})$ positive definite. This implies that the system (35) is parabolic (cf. [36, Chapter 7]).

Acknowledgements

RB is supported by Fondecyt project 1170473; BASAL project CMM, Universidad de Chile and CI^{2}MA, Universidad de Concepción; Fondef ID15I10291; and CRHIAM, Proyecto Conicyt Fondap 15130015.

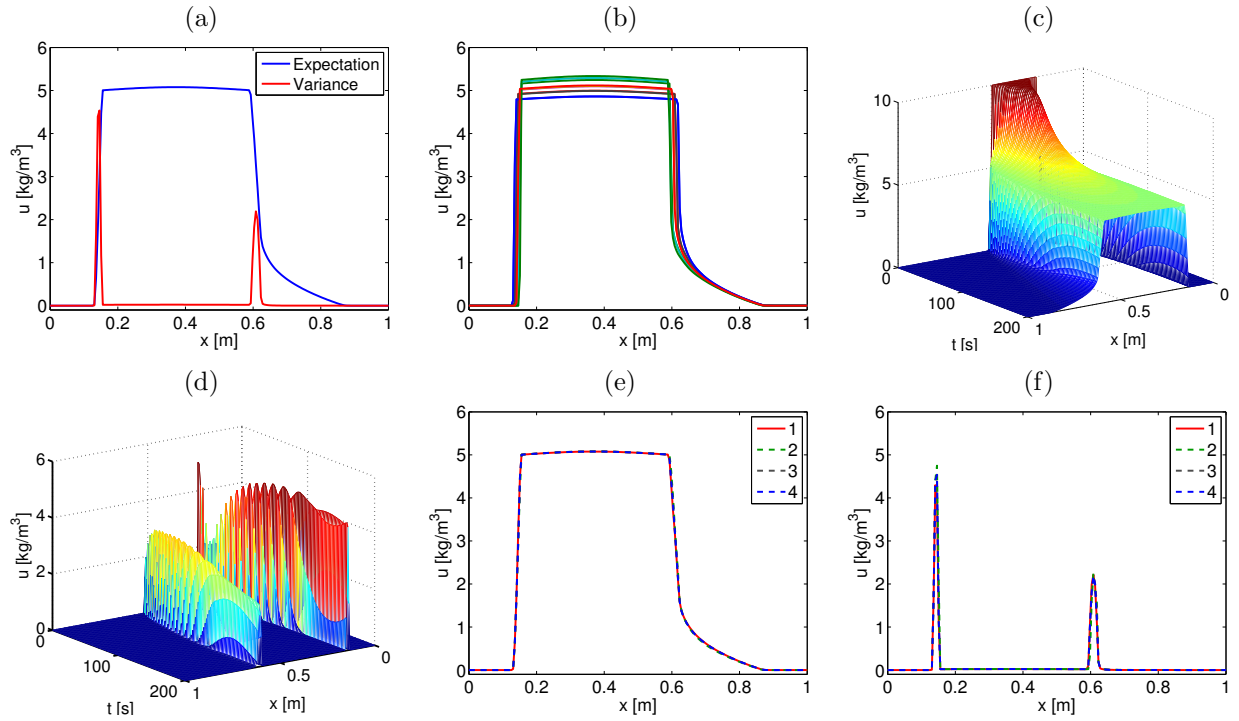

Figure 8: Example 4 (Model 3/Problem C; first setting): numerical solution for $T = 200$ computed with central-upwind and FV-HSG for $N_{\mathrm{r}} = 3$, $N_{\mathrm{o}} = 2$: (a) expectation and variance; (b) reconstructions for 10 several parameter sets; (c) time series of the expectation of the solution for $t \in [0, 200]$; (d) time series of the variance of the solution for $t \in [0, 200]$; (e) comparison of expectations and (f) variance: (1) MC, (2) HSG with $N_{\mathrm{r}} = 2$, $N_{\mathrm{o}} = 1$, (3) HSG with $N_{\mathrm{r}} = 3$, $N_{\mathrm{o}} = 1$, (4) HSG with $N_{\mathrm{r}} = 3$, $N_{\mathrm{o}} = 2$.

IK would like to thank the German Research Foundation (DFG) for financial support of the project within the Cluster of Excellence in Simulation Technology (EXC 310/1) at the University of Stuttgart.

References

[1] C. Acosta, R. Bürger, and C. Mejía. Efficient parameter estimation in a macroscopic traffic flow model by discrete mollificatio. *Transportmetrica A: Transp. Sci.*, 11:702–715, 2015.

[2] B. K. Alpert. Wavelets and other bases for fast numerical linear algebra. In *Wavelets*, volume 2 of *Wavelet Anal. Appl.*, pages 181–216. Academic Press, Boston, MA, 1992.

[3] B. K. Alpert. A class of bases in L^2 for the sparse representation of integral operators. *SIAM J. Math. Anal.*, 24(1):246–262, 1993.

[4] A. Barth, R. Bürger, I. Kröker, and C. Rohde. Computational uncertainty quantification for a clarifier-thickener model with several random perturbations: A hybrid stochastic Galerkin approach. *Computers & Chemical Engineering*, 89:11 – 26, 2016.

[5] A. Barth, C. Schwab, and N. Zollinger. Multi-level Monte Carlo finite element method for elliptic PDEs with stochastic coefficients. *Numer. Math.*, 119(1):123–161, 2011.

[6] R. Bürger and S. Diehl. Convexity-preserving flux identification for scalar conservation laws modelling sedimentation. *Inverse Problems*, 29(4):045008, 2013.

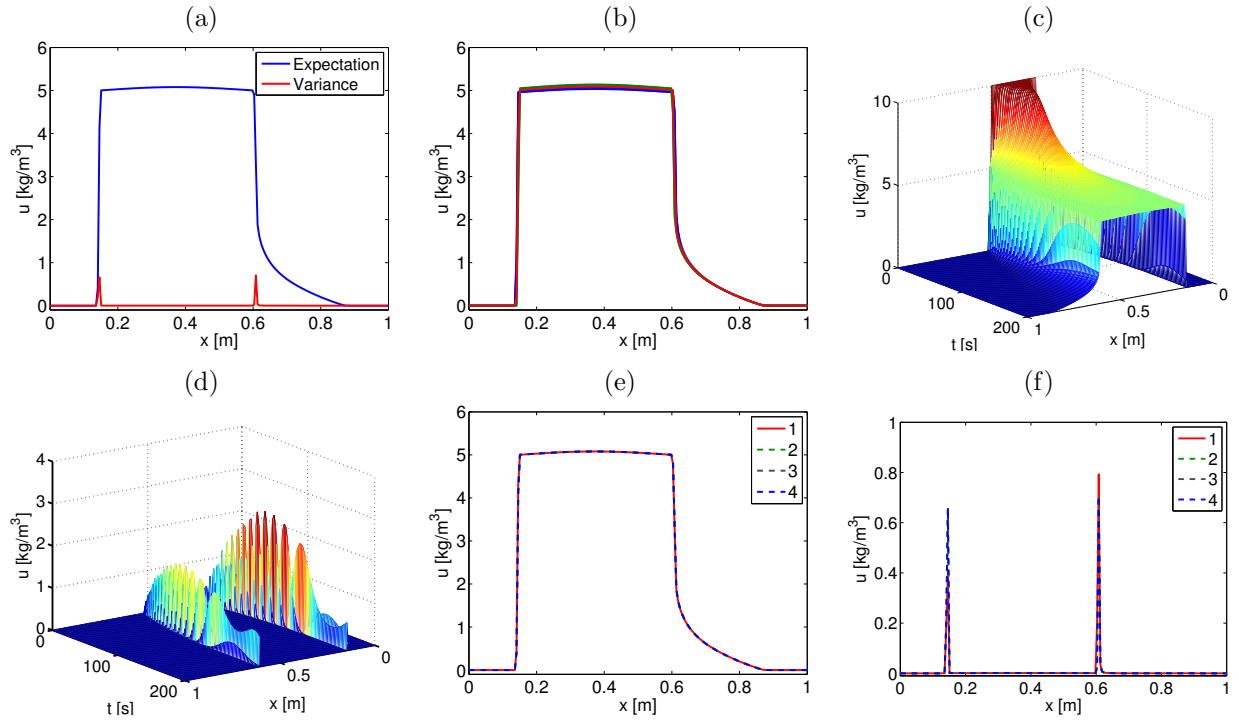

Figure 9: Example 4 (Model 3/Problem C; second setting): numerical solution for $T = 200$ computed with central-upwind and FV-HSG for $N_{\mathrm{r}} = 3$, $N_{\mathrm{o}} = 2$: (a) expectation and variance; (b) reconstructions for 10 several parameter sets; (c) time series of the expectation of the solution for $t \in [0, 200]$; (d) time series of the variance of the solution for $t \in [0, 200]$; (e) comparison of expectations and (f) variance: (1) MC, (2) HSG with $N_{\mathrm{r}} = 2$, $N_{\mathrm{o}} = 1$, (3) HSG with $N_{\mathrm{r}} = 3$, $N_{\mathrm{o}} = 1$, (4) HSG with $N_{\mathrm{r}} = 3$, $N_{\mathrm{o}} = 2$.

[7] R. Bürger, S. Diehl, S. Farås, I. Nopens, and E. Torfs. A consistent modelling methodology for secondary settling tanks: a reliable numerical method. *Water Sci. Tech*, 86:192–208, 2013.

[8] R. Bürger and K. Karlsen. On a diffusively corrected kinematic-wave traffic model with changing road surface conditions. *Math. Models Methods Appl. Sci.*, 13:1767–1799, 2003.

[9] R. Bürger, K. H. Karlsen, and J. D. Towers. Mathematical model and numerical simulation of the dynamics of flocculated suspensions in clarifier–thickeners. *Chemical Engineering Journal*, 111(2–3):119–134, 2005.

[10] R. Bürger, K. H. Karlsen, and J. D. Towers. A model of continuous sedimentation of flocculated suspensions in clarifier-thickener units. *SIAM J. Appl. Math.*, 65(3):882–940, 2005.

[11] R. Bürger, I. Kröker, and C. Rohde. Uncertainty quantification for a clarifier-thickener model with random feed. In *Finite volumes for complex applications. VI. Problems & perspectives. Volume 1, 2*, volume 4, pages 195–203. Springer, 2011.

[12] R. Bürger, I. Kröker, and C. Rohde. A hybrid stochastic Galerkin method for uncertainty quantification applied to a conservation law modelling a clarifier-thickener unit. *ZAMM Z. Angew. Math. Mech.*, 94(10):793–817, 2014.

[13] R. Bürger, W. L. Wendland, and F. Concha. Model equations for gravitational sedimentation-consolidation processes. *ZAMM Z. Angew. Math. Mech.*, 80:79–92, 2000.

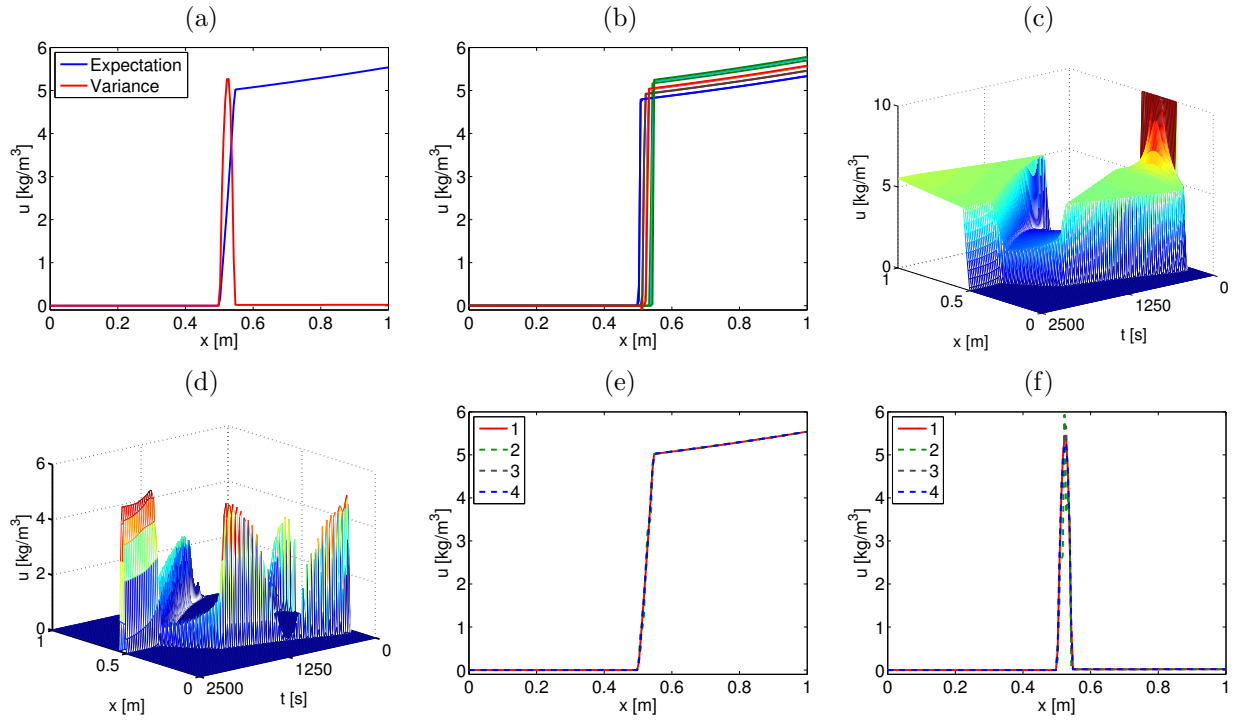

Figure 10: Example 4 (Model 3 / Problem C (first setting)): numerical solution for $T = 2500$ computed with central-upwind and FV-HSG for $N_{\mathrm{r}} = 3$, $N_{\mathrm{o}} = 1$: (a) expectation and variance; (b) reconstructions for 10 several parameter sets; (c) expectation of the solution for $t \in [0, 2500]$; (d) variance of the solution for $t \in [0, 2500]$; (e, f) comparison of (e) expectations and (f) variance: (1) MC, (2) HSG with $N_{\mathrm{r}} = 1$, $N_{\mathrm{o}} = 1$, (3) HSG with $N_{\mathrm{r}} = 2$, $N_{\mathrm{o}} = 1$, (4) HSG with $N_{\mathrm{r}} = 3$, $N_{\mathrm{o}} = 1$.

[14] M. C. Bustos, F. Concha, R. Bürger, and E. M. Tory. *Sedimentation and thickening*, volume 8 of *Mathematical Modelling: Theory and Applications*. Kluwer Academic Publishers, Dordrecht, 1999. Phenomenological foundation and mathematical theory.

[15] J. D. Clercq, I. Nopens, J. Defrancq, and P. A. Vanrolleghem. Extending and calibrating a mechanistic hindered and compression settling model for activated sludge using in-depth batch experiments. *Water Research*, 42(3):781 – 791, 2008.

[16] S. Diehl. A conservation law with point source and discontinuous flux function modelling continuous sedimentation. *SIAM J. Appl. Math.*, 56(2):388–419, 1996.

[17] S. Diehl. Numerical identification of constitutive functions in scalar nonlinear convection-diffusion equations with application to batch sedimentation. *Appl. Numer. Math.*, 95:154–172, 2015.

[18] R. G. Ghanem and P. D. Spanos. *Stochastic finite elements: a spectral approach*. Springer-Verlag, New York, 1991.

[19] B. Greenshields. A study of traffic capacity. *Highway Res. Board Proc*, 14:448–477, 1935.

[20] J. R. Kamm, W. J. Rider, V. G. Weirs, S. Tarantola, and M. Ratto. Sensitivity and uncertainty quantification techniques applied to systems of conservation laws. *Procedia - Social and Behavioral Sciences*, 2(6):7686 – 7687, 2010. Sixth International Conference on Sensitivity Analysis of Model Output.

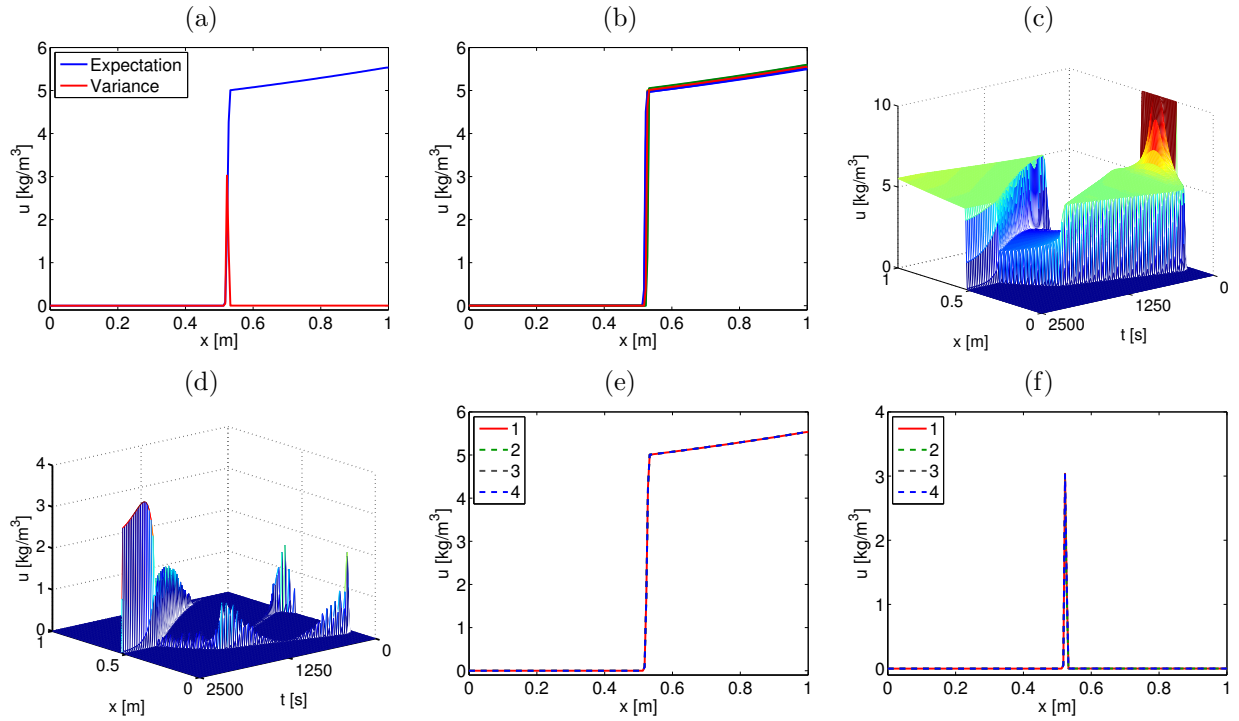

Figure 11: Example 5 (Model 3/Problem C (second setting)): numerical solution for $T = 2500$ computed with central-upwind and FV-HSG for $N_{\mathrm{r}} = 3$, $N_{\mathrm{o}} = 1$: (a) expectation and variance; (b) reconstructions for 10 several parameter sets; (c) expectation of the solution for $t \in [0, 2500]$; (d) variance of the solution for $t \in [0, 2500]$; (e, f) comparison of (e) expectations and (f) variance: (1) MC, (2) HSG with $N_{\mathrm{r}} = 1$, $N_{\mathrm{o}} = 1$, (3) HSG with $N_{\mathrm{r}} = 2$, $N_{\mathrm{o}} = 1$, (4) HSG with $N_{\mathrm{r}} = 3$, $N_{\mathrm{o}} = 1$.

[21] M. Köppel, I. Kröker, and C. Rohde. Stochastic modeling for heterogeneous two-phase flow. In J. Fuhrmann, M. Ohlberger, and C. Rohde, editors, *Finite Volumes for Complex Applications VII-Methods and Theoretical Aspects*, volume 77 of *Springer Proceedings in Mathematics & Statistics*, pages 353–361. Springer International Publishing, 2014.

[22] I. Kröker, W. Nowak, and C. Rohde. A stochastically and spatially adaptive parallel scheme for uncertain and nonlinear two-phase flow problems. *Computational Geosciences*, pages 1–16, 2015.

[23] A. Kurganov and G. Petrova. Central-upwind schemes on triangular grids for hyperbolic systems of conservation laws. *Numerical Methods for Partial Differential Equations*, 21(3):536–552, 2005.

[24] A. Kurganov and E. Tadmor. New high-resolution central schemes for nonlinear conservation laws and convection-diffusion equations. *J. Comput. Phys.*, 160(1):241–282, 2000.

[25] O. P. Le Maître, H. N. Najm, R. G. Ghanem, and O. M. Knio. Multi-resolution analysis of Wiener-type uncertainty propagation schemes. *J. Comput. Phys.*, 197(2):502–531, 2004.

[26] M. Lighthill and G. Whitham. On kinematic waves: Ii. a theory of traffic flow on long crowded roads. *Proc. Roy. Soc. A*, 229:317–345, 1955.

[27] H. G. Matthies and A. Keese. Galerkin methods for linear and nonlinear elliptic stochastic partial differential equations. *Comput. Methods Appl. Mech. Engrg.*, 194(12-16):1295–1331, 2005.

[28] S. Mishra and C. Schwab. Sparse tensor multi-level Monte Carlo finite volume methods for hyperbolic conservation laws with random initial data. *Math. Comp.*, 81(280):1979–2018, 2012.

[29] P. Nelson. Synchronized traffic flow from a modified lighthill-whitham mode. *Phys. Rev. E*, 61:R6052–R6055, 2000.

[30] P. Nelson. Traveling-wave solutions of the diffusively corrected kinematic-wave model. *Math. Comput. Modelling*, 35:561–579, 2002.

[31] G. Poëtte, B. Després, and D. Lucor. Uncertainty quantification for systems of conservation laws. *J. Comput. Phys.*, 228(7):2443–2467, 2009.

[32] P. Richards. Shock waves on the highway. *Oper. Res*, 4:42–51, 1956.

[33] J. F. Richardson and W. N. Zaki. Sedimentation and fluidization: Part i. *Trans. Instn. Chem. Engrs. (London)*, 32:35–53, 1954.

[34] E. Rouvre and G. Gagneux. Solution forte entropique de lois scalaires hyperboliques-paraboliques dégénérées. *C. R. Acad. Sci. Paris Sér. I*, 329:599–602, 1999.

[35] C.-W. Shu and S. Osher. Efficient implementation of essentially nonoscillatory shock-capturing schemes. *J. Comput. Phys.*, 77(2):439–471, 1988.

[36] M. E. Taylor. *Pseudodifferential operators and nonlinear PDE*, volume 100 of *Progress in Mathematics*. Birkhäuser Boston, Inc., Boston, MA, 1991.

[37] J. Tryoen, O. Le Maître, M. Ndjinga, and A. Ern. Intrusive Galerkin methods with upwinding for uncertain nonlinear hyperbolic systems. *J. Comput. Phys.*, 229(18):6485–6511, 2010.

[38] L. Verdickt, I. Smets, and J. V. Impe. Sensitivity analysis of a one-dimensional convection-diffusion model for secondary settling tanks. *Chemical Engineering Communications*, 192(12):1567–1585, 2005.

[39] P. A. Vesilind. Design of prototype thickeners from batch settling tests. *Water Sewage Works*, 115(7):302–307, 1968.

[40] G. Wang and C. Ge. Semidiscrete central-upwind scheme for conservation laws with a discontinuous flux function in space. *Appl. Math. Comput.*, 217(17):7065–7073, 2011.

Centro de Investigación en Ingeniería Matemática (CI^{2}MA)

PRE-PUBLICACIONES 2017

2017-08 Raimund Bürger, Sudarshan K. Kenettinkara, Ricardo Ruiz-Baier, Hector Torres: *Non-conforming/DG coupled schemes for multicomponent viscous flow in porous media with adsorption*

2017-09 Thomas Führer, Norbert Heuer, Michael Karkulik, Rodolfo Rodríguez: *Combining the DPG method with finite elements*

2017-10 Cinthya Rivas, Rodolfo Rodríguez, Manuel Solano: *A perfectly matched layer for finite-element calculations of diffraction by metallic surface-relief gratings*

2017-11 Raimund Bürger, Pep Mulet, Lihki Rubio, Mauricio Sepúlveda: *Linearly implicit IMEX schemes for the equilibrium dispersive model of chromatography*

2017-12 Veronica Anaya, Zoa De Wijn, David Mora, Ricardo Ruiz-Baier: *Mixed displacement-rotation-pressure formulations for elasticity*

2017-13 Veronica Anaya, David Mora, Carlos Reales, Ricardo Ruiz-Baier: *A vorticity-pressure finite element formulation for the Brinkman-Darcy coupled problem*

2017-14 Mario Álvarez, Gabriel N. Gatica, Ricardo Ruiz-Baier: *A posteriori error analysis of a fully-mixed formulation for the Brinkman-Darcy problem*

2017-15 Daniele Boffi, Lucia Gastaldi, Rodolfo Rodríguez, Ivana Sebestova: *A posteriori error estimates for Maxwell eigenvalue problem*

2017-16 Gabriel N. Gatica: *A note on weak* convergence and compactness and their connection to the existence of the inverse-adjoint*

2017-17 Eligio Colmenares, Gabriel N. Gatica, Ricardo Oyarzúa: *A posteriori error analysis of an augmented fully-mixed formulation for the stationary Boussinesq model*

2017-18 Javier A. Almonacid, Gabriel N. Gatica, Ricardo Oyarzúa: *A mixed-primal finite element method for the Boussinesq problem with temperature-dependent viscosity*

2017-19 Raimund Bürger, Ilja Kröker: *Computational uncertainty quantification for some strongly degenerate parabolic convection-diffusion equations*

Para obtener copias de las Pre-Publicaciones, escribir o llamar a: Director, Centro de Investigación en Ingeniería Matemática, Universidad de Concepción, Casilla 160-C, Concepción, Chile, Tel.: 41-2661324, o bien, visitar la página web del centro: `http://www.ci2ma.udec.cl`







Centro de Investigación en
Ingeniería Matemática (CI²MA)
Universidad de Concepción

Casilla 160-C, Concepción, Chile
Tel.: 56-41-2661324/2661554/2661316
http://www.ci2ma.udec.cl